

Experimental Determination of the Absolute Enantioselectivity of an Antibody-Catalyzed Diels–Alder Reaction and Theoretical Explorations of the Origins of Stereoselectivity

Carina E. Cannizzaro, Jon A. Ashley, K. D. Janda, and K. N. Houk*

Contribution from the Department of Chemistry and Biochemistry, University of California, Los Angeles, California 90095-1569, and Department of Chemistry and the Skaggs Institute for Chemical Biology, The Scripps Research Institute, La Jolla, California 92037

Received June 24, 2002; E-mail: houk@chem.ucla.edu

Abstract: The *exo* and *endo* Diels–Alder adducts of *p*-methoxycarbonylbenzyl *trans*-1,3-butadiene-1-carbamate and *N,N*-dimethylacrylamide have been synthesized, and the absolute configurations of resolved enantiomers have been determined. On the basis of this information, the absolute enantioselectivities of the Diels–Alder reaction catalyzed by antibodies **13G5** and **4D5** as well as other catalytic antibodies elicited in the same immunizations have been established. The effects of different arrangements of catalytic residues on the structure and energetics of the possible Diels–Alder transition states were modeled quantum mechanically at the B3LYP/6-311++G**//B3LYP/6-31+G** level of theory. Flexible docking of these enantiomeric transition states in the antibody active site followed by molecular dynamics on the resulting complexes provided a prediction of the transition-state binding modes and an explanation of the origin of the observed enantioselectivity of antibody **13G5**.

Introduction

The Diels–Alder reaction is one of the most powerful carbon–carbon bond-forming processes in organic chemistry. For many synthetic applications, the value of the Diels–Alder reaction resides in the degree of stereocontrol that can be exercised. Extensive efforts have been focused on controlling the diastereo- and enantioselectivity of the Diels–Alder reaction.¹ Some chiral Lewis acids effectively catalyze the [4 + 2] cycloaddition reactions of various dienes and dienophiles,¹ while simple organic amine catalysts have been developed recently to catalyze Diels–Alder reactions of different dienes with α,β -unsaturated aldehydes.² Several systems have also been reported that accelerate the Diels–Alder reaction by noncovalent catalysis, that is, by presenting a host cavity complementary to the transition state. These include micelles,³ bovine serum albumin,⁴ Baker's yeast,⁵ cyclodextrins,⁶ Rebek's tennis ball,⁷

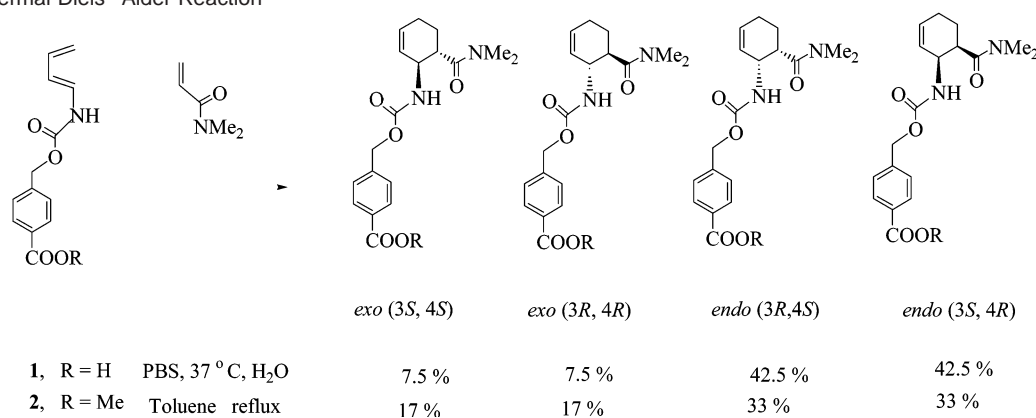
and synthetic RNA fragments.⁸ There are proposals that enzyme-catalyzed Diels–Alder reactions may occur during biosynthesis of several secondary metabolites.^{9–12}

Antibodies have been successful in catalyzing several types of Diels–Alder reaction.¹³ Antibodies have attracted attention because catalysis is not limited to metabolically important reactions¹⁴ and might be developed for a broad range of organic reactions.

- (1) Recent reviews of enantioselective Lewis acid-catalyzed Diels–Alder reactions: (a) Togni, A.; Venanzi, L. M.; *Angew. Chem., Int. Ed. Engl.* **1994**, *33*, 497–526. (b) Maruoka, K.; Yamamoto, H. In *Catalytic Asymmetric Synthesis*; Ojima, I., Ed.; VCH: New York, 1993; Chapter 9. (c) Pindur U.; Lutz, G.; Otto, C. *Chem. Rev.* **1993**, *93*, 741–761. (d) Deloux, L.; Srebnik, M. *Chem. Rev.* **1993**, *93*, 763–784. (e) Kagan, H. B.; Riant, O. *Chem. Rev.* **1992**, *92*, 1007–1019.
- (2) Ahrendt, K. A.; Borths, C. J.; MacMillan, W. C. *J. Am. Chem. Soc.* **2000**, *122*, 4243–4244.
- (3) Braun, R.; Schuster, F.; Sauer, J. *Tetrahedron Lett.* **1986**, *27*, 1285–1288.
- (4) Colonna, S.; Manfredi, A.; Annunziata, R. *Tetrahedron Lett.* **1988**, *29*, 3347–3350.
- (5) Rao, K. R.; Srinivasan, T. N.; Bhanumathi, N. *Tetrahedron Lett.* **1990**, *31*, 5959–5960.
- (6) (a) Hudlicky, T.; Butora, G.; Fearnley, S. P.; Gum, A. G.; Persichini, P. J., III; Stabile, M. R.; Merola, J. S. *J. Chem. Soc., Perkin Trans. 1* **1995**, *19*, 2393–2398. (b) Alvira, E.; Cattivola, C.; Garcia, J. I.; Mayoral, J. A. *Tetrahedron Lett.* **1995**, *36*, 2129–2132. (c) Sternbach, D. D.; Rossana, D. M. *J. Am. Chem. Soc.* **1982**, *104*, 5853–5854.
- (7) Kang, J.; Santamaria, J.; Hilmersson, G.; Rebek, J., Jr. *J. Am. Chem. Soc.* **1998**, *120*, 7389–7390.

- (8) (a) Morris, K. N.; Tarasow, T. M.; Julin, C. M.; Simons, S. L.; Hilvert, D.; Gold, L. *Proc. Natl. Acad. Sci. U.S.A.* **1994**, *91*, 13028–13032. (b) Seelig, B.; Jaschke, A. *Chem. Biol.* **1999**, *6*, 167–176. (c) Tarasow, T. M.; Eaton, B. E. *J. Am. Chem. Soc.* **2000**, *122*, 1015–1021.
- (9) Ichihara, A.; Oikawa, H. In *Comprehensive Natural Products Chemistry*; Sankawa, U., Ed.; Barton, D., Nakanishi, K., Met-Cohn, O., Series Eds.; Polyketides and Other Secondary Metabolites, Vol. 1; Elsevier: New York, 1999; pp 367–408.
- (10) (a) Pohnert, G. *ChemBioChem* **2001**, *2*, 873–875. (b) Auclair, K.; Sutherland, A.; Kennedy, J.; Witter, D. J.; Van den Heever, J. P.; Hutchinson, C. R.; Vederas, J. C. *J. Am. Chem. Soc.* **2000**, *122*, 11519–11520. (c) Hutchinson, C. R.; Kennedy, J.; Park, C.; Kendrew, S.; Auclair, K.; Vederas, J. *Antonie van Leeuwenhoek* **2000**, *78*, 287–295.
- (11) (a) Oikawa, H.; Katayama, K.; Suzuki, Y.; Ichihara, A. *J. Chem. Soc., Chem. Commun.* **1995**, 1321–1322. (b) Oikawa, H.; Kobayashi, T.; Katayama, K.; Suzuki, Y.; Ichihara, A. *J. Org. Chem.* **1998**, *63*, 8748–8756. (c) Katayama, K.; Kobayashi, T.; Oikawa, H.; Honma, M.; Ichihara, A. *Biochim. Biophys. Acta* **1998**, *1384*, 387–395. (d) Oikawa, H.; Suzuki, Y.; Katayama, K.; Naya, A.; Sakano, C.; Ichihara, A. *J. Chem. Soc., Perkin Trans. 1* **1999**, 1225–1232.
- (12) (a) Watanabe, K.; Mie, T.; Ichihara, A.; Oikawa, H.; Honma, M. *J. Biol. Chem.* **2000**, *275*, 287–295. (b) For a recent review on Diels–Alderase: Pohnert, G. *ChemBioChem* **2001**, *2*, 873–875.
- (13) (a) Hilvert, D.; Hill, K. W.; Nared, K. D.; Auditor, M. M. *J. Am. Chem. Soc.* **1989**, *111*, 1, 9261–9262. (b) Braisted, A. C.; Schultz, P. G. *J. Am. Chem. Soc.* **1990**, *112*, 7430. (c) Suckling, C. J.; Tedford, M. C.; Bence, L. M.; Irvine, J. I.; Stimson, W. H. *J. Chem. Soc., Perkin Trans. 1* **1993**, 1925. (d) Gouverneur, V. E.; Houk, K. N.; de Pascual-Teresa, B.; Beno, B.; Janda, K. D.; Lerner, R. A. *Science* **1993**, *262*, 204–208. (e) Yli-Kauhala, J. T.; Ashley, J. A.; Lo, C.; Tucker, L.; Wolfe, M. M.; Janda, K. D. *J. Am. Chem. Soc.* **1995**, *117*, 7041–7047. (f) Meekel, A. P.; Resmini, M.; Pandit, U. K. *J. Chem. Soc., Chem. Commun.* **1995**, 571–572. (g) Resmini, M.; Meekel, A. P.; Pandit, U. K. *Pure Appl. Chem.*, **1996**, *68*, 2025–2028.

Scheme 1. Thermal Diels–Alder Reaction



Electron-rich dienes, such as alkoxy- or amino-substituted dienes are especially valuable in synthesis,¹⁵ and Cr(III)–salen complexes¹⁶ have been developed for the enantioselective catalysis of the Diels–Alder reaction of such dienes.

A reaction of this type that has been catalyzed by antibodies involves the cycloaddition of amino-substituted diene **1** and *N,N*-dimethyl acrylamide (Scheme 1). Regioselectivity is high, and only four ortho isomers shown in the scheme are observed experimentally. To obtain only one adduct out of the four possible isomers, the reaction must be both diastereoselective (*endo*–*exo*) and enantioselective. This level of selection represents a great challenge to any particular catalyst.

In 1993, antibodies **22C8** and **7D4** were elicited against racemic, bis-cyclooctene transition-state (TS) analogues, shown in Figure 1a.^{13d} Whereas the thermal reaction is only slightly *endo* selective (Scheme 1), the antibodies catalyze enantioselectively the formation of one enantiomer of the *exo* (trans) and one enantiomer of the *endo* (cis) adducts, respectively.

Two years later, antibodies **13G5** and **4D5** were raised to flexible ferrocene haptens, shown in Figure 1b.^{13e} Indirect comparison of the chiral HPLC retention times of the products obtained with both sets of antibodies revealed that **13G5** and **4D5** catalyzed the formation of the same *exo* and *endo* adducts, respectively. No studies of the absolute configuration of these products were undertaken. Computational modeling that involved locating gas-phase transition states followed by docking into the crystal structure of **13G5** with Autodock V2.4 showed that the four possible transition states can be accommodated in the active site. Only the *exo* transition states maintained the hydrogen-bonding motif observed in the crystal structure of an inhibitor bound to *exo*-Diels–Alderase **13G5**.¹⁷ It was suggested that the *exo*-(3*R*,4*R*) transition structure is the most highly stabilized but that definitive evidence could only be obtained by determination of the absolute configuration of the product obtained from **13G5** catalysis.¹⁷

To improve the modest catalytic acceleration by these antibodies (for example **13G5** has: $k_{\text{cat}} = 1.2 \times 10^{-3} \text{ min}^{-1}$;

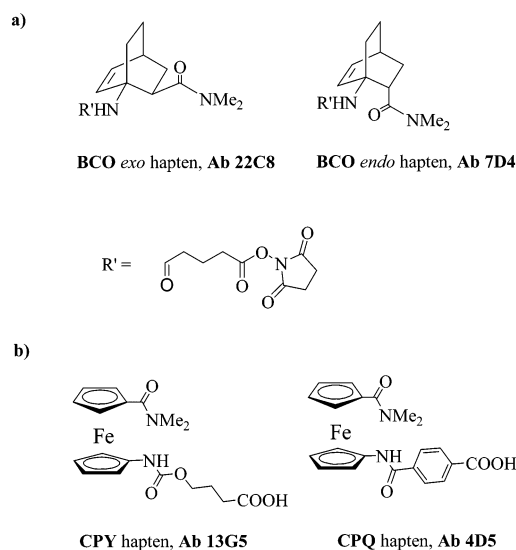


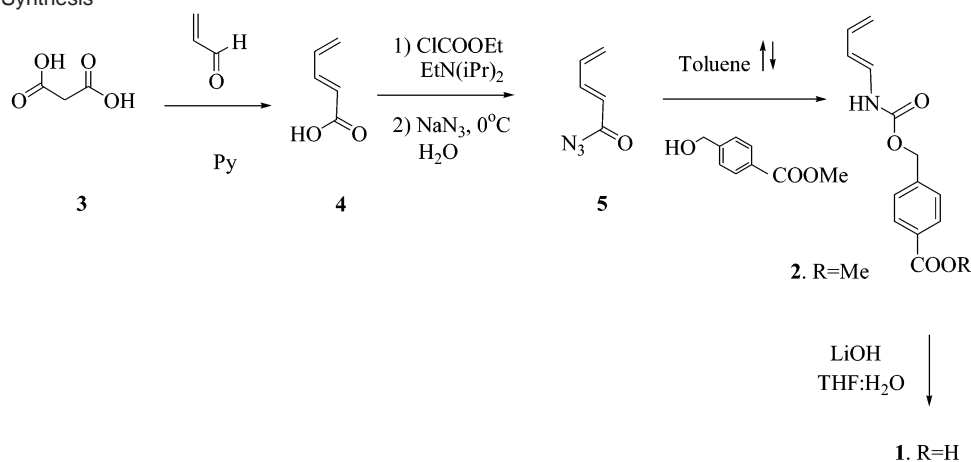
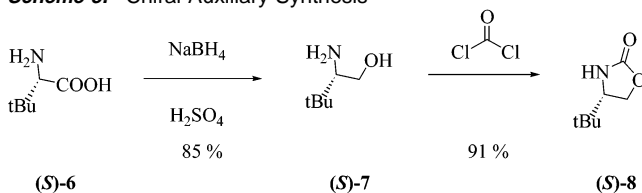
Figure 1. Racemic haptens for the Diels–Alder reaction.

$k_{\text{cat}}/k_{\text{uncat}} = 6.9 \text{ M}$) requires a good understanding of the interactions responsible for catalysis in the active site. To program antibodies to catalyze the formation of each of the four possible ortho adducts, a thorough understanding of the factors determining the enantioselectivity is necessary.

We have now synthesized and established the absolute configuration of the products obtained by antibody catalysis with **13G5**, **4D5**, and 15 other catalytic antibodies elicited for the reaction in Scheme 1. The enantioselectivity of several of these antibodies has been established experimentally, and some considerations are made as to the origins of stereoselectivity occurring by these antibodies, elicited to achiral or racemic haptens. The reaction has been studied quantum mechanically at a higher level of theory than previously, and the effects of different arrangements of catalytic residues on the structure and energetics of the possible transition states have been determined. Flexible docking of these transition states in the antibody active site, followed by molecular dynamical studies of the resulting complexes, led to an explanation of the observed enantioselectivity of antibody **13G5**.

Preparation of the Enantiomerically Pure Diels–Alder Adducts and Determination of Their Absolute Stereochemistries. Synthetic Methodology. Diene **2** undergoes cycloaddition with *N,N*-dimethylacrylamide at 110 °C in refluxing toluene to afford a mixture of the stereoisomeric *endo* (cis) and

- (14) (a) Wentworth, P., Jr.; Janda, K. D. *Cell Biochem. Biophys.* **2001**, *35*, 63–87. (b) Tremblay, M. R.; Dickerson, T. J.; Janda, K. D. *Adv. Synth. Catal.* **2001**, *343*, 577–585 and references therein. (c) Schultz, P. G.; Lerner, R. A. *Science* **1995**, *269*, 1835. (d) Stewart, J. D.; Benkovic, S. J. *Nature* **1995**, *375*, 388–391. (e) Keinan, E.; Lerner, R. A. *Isr. J. Chem.* **1996**, *36*, 113–119. (f) Morrison, J. D., Ed. *Chiral Catalysis; Asymmetric Synthesis*, Vol. 5; Academic Press: New York, 1985.
- (15) Kozmin, S. A.; Rawal, V. H. *J. Am. Chem. Soc.* **1998**, *120*, 13523–13524.
- (16) Huanh, Y.; Iwama, T.; Rawal, V. H. *J. Am. Chem. Soc.* **2000**, *122*, 7843–7844.
- (17) Heine, A.; Stura, E. A.; Yli-Kauhaluoma, J. T.; Gao, C.; Deng, Q.; Beno, B. R.; Houk, K. N.; Janda, K. D. and Wilson, I. A. *Science* **1998**, *279*, 1934–1940.

Scheme 2. Diene Synthesis**Scheme 3.** Chiral Auxiliary Synthesis

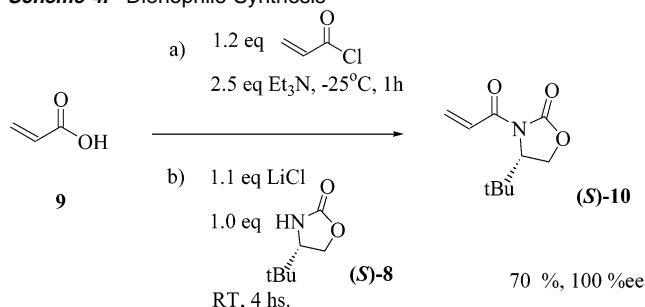
exo (trans) adducts in a ratio of 66:34.¹⁸ When the same reaction is carried out with the water-soluble diene **1** in phosphate-buffered saline (PBS), an 85:15 mixture of the *endo* and *exo* adducts is obtained. Both reactions are completely regioselective, giving only the ortho regioisomers (Scheme 1).

We expected, therefore, that the thermal cycloaddition between diene **2** and dienophile **(S)-10** would give direct access to a separable mixture of the diastereomeric Diels–Alder adducts, one *endo* and one *exo*, bearing a third chiral center of known stereochemistry, a requirement for the unequivocal assignment of the absolute configuration of the adducts by X-ray crystallography in the absence of an anomalous dispersion atom. The selection of the chiral auxiliary was based on the observation that crotonates with *tert*-butyl oxazolidinones as chiral auxiliaries show the highest degree of diastereoselection in the Et_2AlCl -catalyzed Diels–Alder cycloaddition with isoprene; diastereoselectivity is beyond the limits of detection (> 100 ds).¹⁹

Dienes **1** and **2** were synthesized according to a modification of Overman's procedure²⁰ (Scheme 2) described in full in the Supporting Information.

The chiral auxiliary **(S)-8** (Scheme 3) was obtained by reduction of commercially available *(S)*-*tert*-leucine, **(S)-6**, with borane generated in situ²¹ to give the intermediate alcohol **(S)-7**, followed by cyclization with phosgene.²²

The chiral dienophile **(S)-10** was first synthesized by addition of the *(S)*-(-)-4-*tert*-butyl-2-oxazolidinone bromomagnesium salt to 3-bromopropionyl chloride followed by dehydrohalogenation of the resultant 3-bromopropionyl imide with triethylamine, according to the strategy developed by Evans.²³ An

Scheme 4. Dienophile Synthesis

improved methodology by Mathre et al.²⁴ (Scheme 4) involves nucleophilic attack of *(S)*-(-)-4-*tert*-butyl-2-oxazolidinone lithium salt on the previously formed acryloyl anhydride.

The asymmetric Diels–Alder cycloaddition was carried out first between equimolar quantities of diene **2** and dienophile **(S)-10** under the Lewis acid-catalyzed conditions (AlEt_2Cl).^{23,25} Unfortunately, the carbamate moiety was reactive under these conditions, and no Diels–Alder adduct formation was detected. The reaction was carried out successfully without catalyst in refluxing toluene to give *endo*-**11** and *exo*-**11** as diastereomeric pure adducts in a ratio of 67:33 (Scheme 5).

Compound *endo*-**11** was recrystallized from ethyl ether:hexanes (1:1 v/v), and the absolute configuration of the newly created stereocenters was determined by X-ray diffraction analysis. The X-ray structure is shown in Figure 2. From the known *S* configuration of the chiral auxiliary, it is determined that compound *endo*-**11** has the (3*R*,4*S*) configuration. Note the preferred *s-cis* conformation around the O–C bond of the carbamate group (dihedral $\text{O}=\text{C}-\text{O}-\text{C} = 7.7^\circ$). The dihedral angles around the O–C bond of the carbamate ester portion are $+27.2^\circ$ for the *gauche* hydrogen, -93.4° for the methyl benzoate group, and $+146.5^\circ$ for the hydrogen in an *anti* arrangement.

The Evans regioselective hydrogen peroxide-mediated hydrolysis of oxazolidinone-type chiral auxiliaries²⁶ was used for the conversion of *endo*-**11** into *endo*-**12**. Removal of the chiral auxiliary without epimerization or carbamate hydrolysis was performed at a reasonable rate at room temperature using 4 equiv

(18) Overman, L. E.; Taylor, G. F.; Petty, C. B.; Jessup, P. J. *J. Org. Chem.* **1978**, *43*, 2164.

(19) Evans, D. A.; Chapman, K. T.; Hung, D. T.; Kawaguchi, A. T. *Angew. Chem., Int. Ed. Engl.* **1987**, *26*, 1184–1186.

(20) Jessup, P. J.; Petty, C. B.; Roos, J.; Overman, L. E. *Organic Syntheses*; Wiley: New York, 1988; Collect. Vol. VI, p 95.

(21) Abiko, A.; Masamune, S. *Tetrahedron Lett.* **1992**, *33*, 5517–5518.

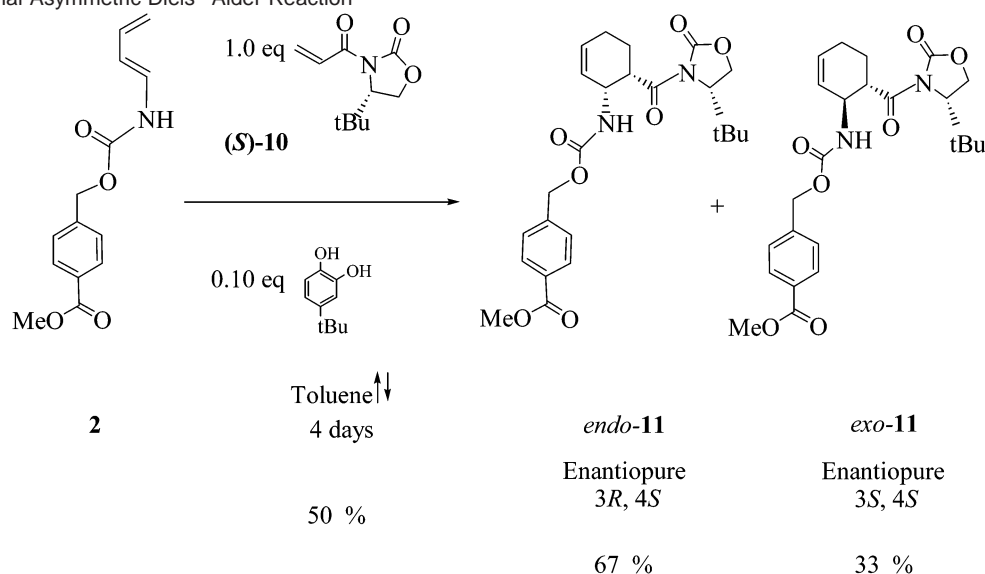
(22) Newman, M. S.; Kutner, A. *J. Am. Chem. Soc.* **1951**, *73*, 4199–4204.

(23) Evans, D. A.; Chapman, K. T.; Bisaha, J. *J. Am. Chem. Soc.* **1988**, *110*, 1238–1256.

(24) Mathre, D. J.; Ho, G.-J. *J. Org. Chem.* **1995**, *60*, 2271–2273.

(25) Gawley, R. E.; Aubé J. *Principles of Asymmetric Synthesis*; Pergamon: Oxford, 1996; p 263.

(26) Evans, D. A.; Britton, T. C.; Ellman, J. A. *Tetrahedron Lett.* **1987**, *28*, 6141–6144.

Scheme 5. Thermal Asymmetric Diels–Alder Reaction

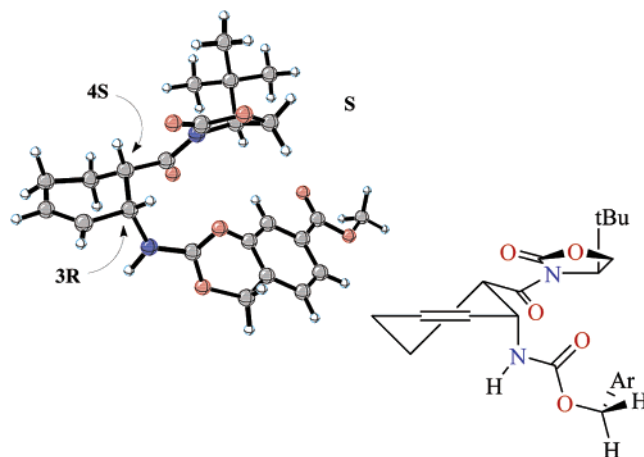
of hydrogen peroxide and 2 equiv of LiOH. The desired acid, *endo-12*, was obtained in 95% yield, based upon 81% conversion.

Palladium-catalyzed hydrogenation of the double bond followed by hydrogenolysis of the carbamate moiety^{27–29} of acid *endo-12* gave β -amino acid *endo-15*. The absolute stereochemistry of this β -amino acid derivative, and therefore of *endo-12*, was determined by comparing its optical rotation $[\alpha]^{20}_D = +2.0$ ($c = 0.20$ in methanol) with literature values of $[\alpha]^{25}_D = +1.7$ ($c = 0.60$ in water) for the corresponding hydrochloride.³⁰ This experiment proved that no significant epimerization had occurred during removal of the chiral auxiliary (optical rotation of the 3*R*,4*R* epimer: $[\alpha]^{25}_D = -45.4$ ($c = 1.04$ in water) for the corresponding hydrochloride,³⁰ and $[\alpha]^{16}_D = -65.5$ ($c = 2$ in water) for the neutral compound³³) and also provided an alternative method for the determination of the absolute configuration of the *exo* adduct.

Amidation of acid *endo-12* was carried out successfully by activation with carbonyl diimidazole followed by addition of dimethylamine as reported by Jung et al.³¹ Amide *endo-13* was obtained in 82% crude yield. Final hydrolysis of the methyl ester gave the *endo-14* final target in 98% yield with the 3*R*,4*S* configuration (Scheme 6).

We attempted to prepare the *exo*-(3*R*,4*R*) adduct by epimerization of the enantiomerically pure *endo*-(3*R*,4*S*) adduct with 4 equiv of potassium *tert*-butoxide in *tert*-butyl alcohol at room temperature. However, ¹H 500 MHz NMR analysis of each spot showed no signs of epimerization. Starting material, *p*-hydroxymethylbenzoic acid, and decomposed material were found.

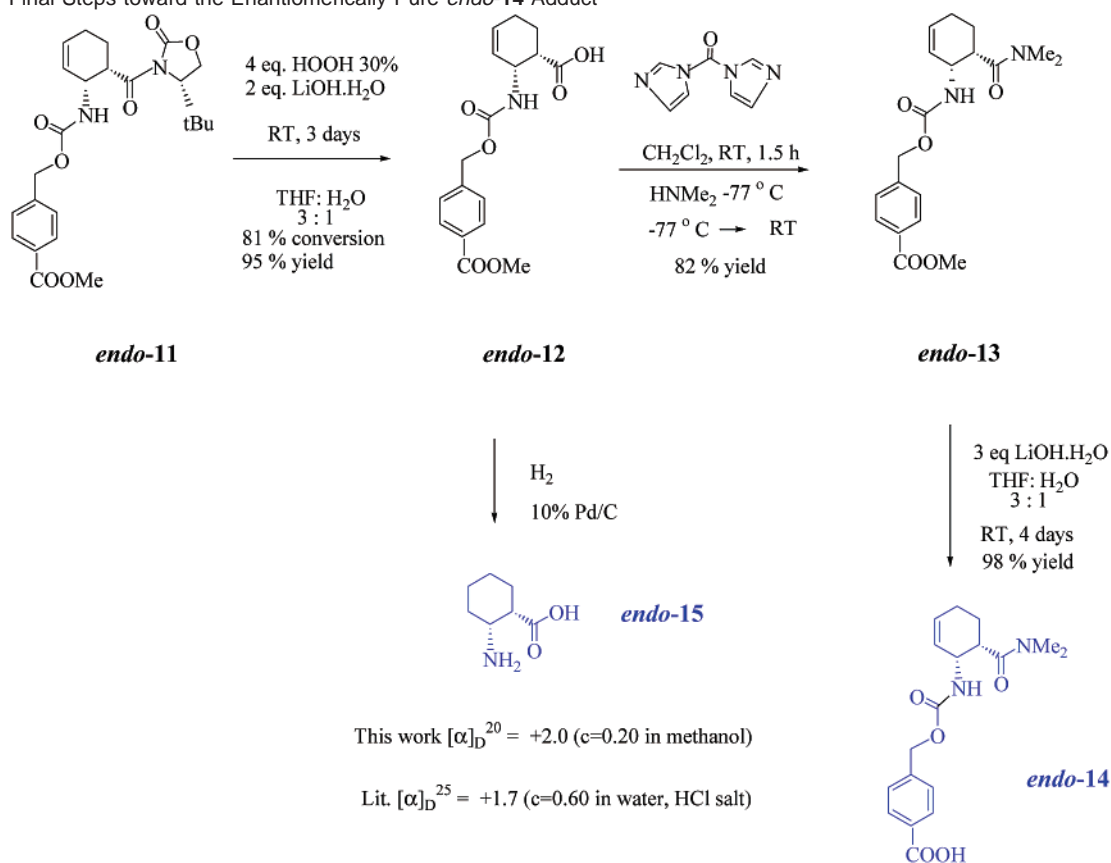
We explored the equilibrium between the *exo*-(3*R*,4*R*) and *endo*-(3*R*,4*S*) adducts with semiempirical AM1 calculations summarized in Scheme 7. The *endo* (cis) conformer with the

**Figure 2.** X-ray crystal structure of *endo-11* adduct.

carbamate group axial and the dimethylamide equatorial is most stable and should be present to the extent of about 90% at equilibrium at room temperature due to A^{1,3} strain involving the carbamate. These computations explain why epimerization does not readily give the *trans* isomer. Efforts were then directed toward the isolation of the *exo-11* adduct obtained along with *endo-11* adduct from the thermal Diels–Alder reaction mixture. Four consecutive column chromatographies were necessary to isolate approximately 0.7 g of pure *exo-11* adduct by NMR. Attempts to recrystallize this glassy material were unsuccessful. An analytical sample of this material was further purified by HPLC, but crystallization remained elusive. To establish the absolute stereochemistry of the pure *exo-11* adduct and obtain a sample of the final *exo* product, we followed the same synthetic route developed for the *endo-11* adduct. Transformation of *exo-11* into *exo-12* was carried out successfully, and the acid was isolated as an amorphous white solid (Scheme 8).

Treatment of the acid *exo-12* with the different optically active amines, (+)-(2*S*,3*R*)-4-(dimethylamino)-3-methyl-1,2-diphenyl-2-butanol or (*R*)-methylbenzylamine, gave needle-shaped crystals that were too small to produce a useful diffraction pattern in either case. Since crystallization failed, we turned to chemical correlation. The β -amino acid, *exo-15*, was obtained from a pure

- (27) Jackson, A. E.; Johnstone, R. A. W. *Synthesis* **1976**, 685–687.
 (28) Meienhofer, J.; Kuromizu, K. *Tetrahedron Lett.* **1974**, 37, 3259–3262.
 (29) ElAmin, B.; Anantharamaiah, G. M.; Royer, G. P.; Means, G. E. *J. Org. Chem.* **1979**, 44, 3442–3444.
 (30) Davies, S. G.; Ichihara, O.; Lenoir, I.; Walters, I. A. S. *J. Chem. Soc., Perkin Trans. 1* **1994**, 1411–1415.
 (31) Jung, M. E.; Dámico, D. C. *J. Am. Chem. Soc.* **1995**, 117, 7379–7388.
 (32) Nohira, H.; Ehara, K.; Miyashita, A. *Bull. Chem. Soc. Jpn.* **1970**, 43, 2230–2233.
 (33) (a) Lee, C.; Yang, W.; Parr, R. G. *Phys. Rev. B* **1988**, 37, 785. (b) Becke, A. D. *J. Chem. Phys.* **1993**, 98, 5648.

Scheme 6. Final Steps toward the Enantiomerically Pure *endo*-14 Adduct

sample of *exo*-12 by catalytic hydrogenation of the double bond followed by hydrogenolysis of the carbamate moiety.^{27–29} The absolute stereochemistry of the β -amino acid *exo*-15, and therefore of *exo*-12, was determined by comparing its optical rotation $[\alpha]_{\text{D}}^{20} = +63.0$ ($c = 0.25$ in methanol) with literature values of $[\alpha]_{\text{D}}^{17} = +66.5$ ($c = 2$ in water)³² for the same amino acid, and $[\alpha]_{\text{D}}^{25} = +47.4$ ($c = 1.14$ in water) for the corresponding hydrochloride.³⁰ After amidation of *exo*-12 and hydrolysis of the methyl ester of *exo*-13, the enantiomerically pure *exo*-(3*S*,4*S*)-14 adduct was obtained as an amorphous white solid.

Determination of the Absolute Stereoselectivity of the Diels–Alderase Catalytic Antibodies. The order in which the four isomeric Diels–Alder adducts appear in the chiral HPLC trace was first identified by comparisons with our authentic *exo* and *endo* adducts. The Diels–Alder reaction was then performed in the presence of catalytic amounts of different antibodies, and the mixture of stereoisomeric cycloadducts was analyzed by chiral HPLC (see Supporting Information for details).

Results

Figure 3a shows the chiral HPLC traces of a standard mixture of the four stereoisomers made by combining equal amounts of racemic *endo* and *exo* adducts. Figure 3b is a trace of the enantiomerically pure sample of *exo*-(3*S*,4*S*)-14, and Figure 3c is a trace of the enantiomerically pure sample of *endo*-(3*R*,4*S*)-14.

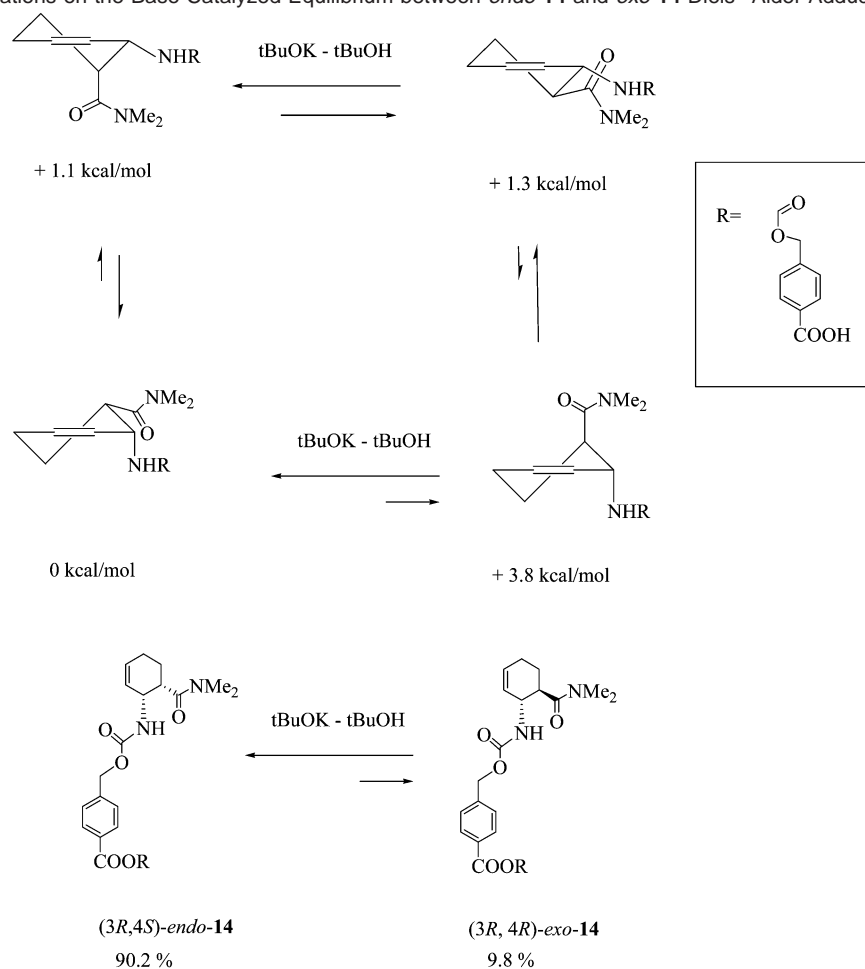
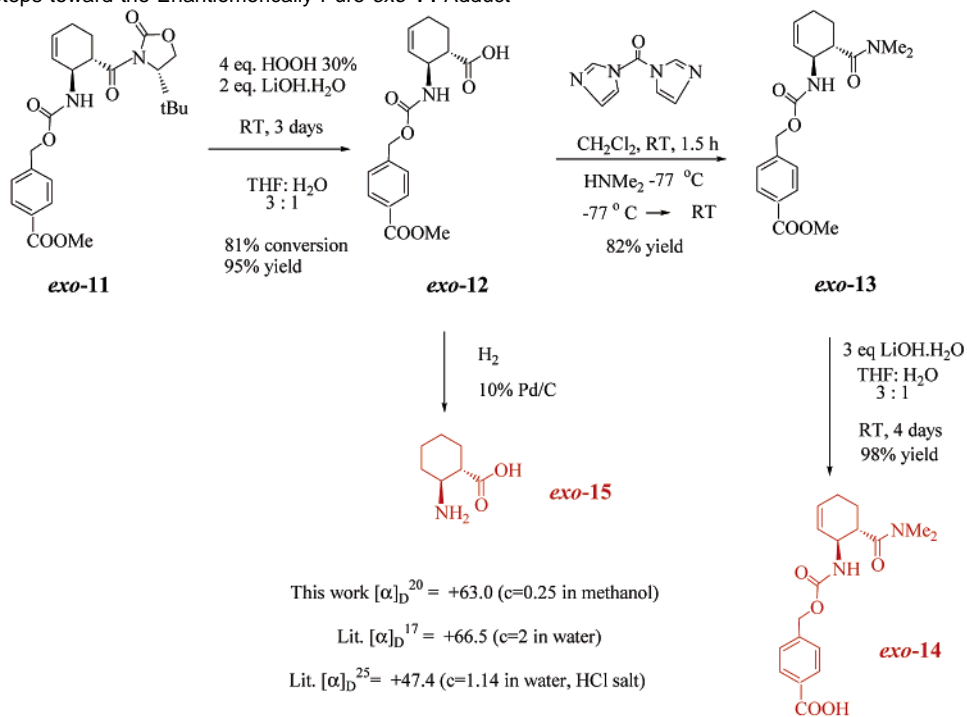
Under the conditions used to separate the four isomers, the first peak corresponds to the *exo*-(3*S*,4*S*) cycloadduct (retention time = 12.15 min), and the fourth peak corresponds to the *endo*-(3*R*,4*S*) adduct (retention time = 21.77 min).

Immunization with the CPY hapten (Figure 1b) had originally produced six *exo*-Diels–Alderases **13G5**, **4D3**, **7G8**, **2A3**, **6D7**, and **14D9**, in order of decreasing effectiveness of catalysis relative to the uncatalyzed reaction, and one *endo*-Diels–Alderase, antibody **2A3**.^{13e} The immune system responded to the CPQ hapten (Figure 1b) to generate seven *endo*-Diels–Alderases **4D5**, **8G2**, **12F10**, **15C1**, **9B4**, **1F4**, and **12D2**, presented again in order of decreasing efficacy of catalysis relative to the uncatalyzed reaction, along with one *exo*-Diels–Alderase, antibody **7D10**.^{13e}

Comparisons of HPLC traces of the enantiomerically pure products and the products of the antibody-catalyzed reactions, showed that antibody **13G5**, the most efficient of all *exo*-Diels–Alderases, catalyzes the formation of the *exo*-(3*S*,4*S*) adduct. All of the other *exo*-Diels–Alderases catalyzed the formation of the same *exo*-(3*S*,4*S*) adduct, regardless of their relative rates of catalysis. Even *exo*-Diels–Alderase **7D10**, elicited to a different hapten (CPQ), also catalyzes the formation of the *exo*-(3*S*,4*S*) adduct. These results are summarized in Table 1.

We also found that all *endo*-Diels–Alderases **4D5**, **8G2**, **12F10**, **15C1**, **9B4**, **1F4**, and **12D2** (from hapten CPQ) and **2A3** (from hapten CPY) catalyzed the formation of the *endo*-(3*R*,4*S*) adduct.

Earlier results^{4e} showed that *exo*-Diels–Alderase **22C8**, elicited from the bicyclooctene hapten, BCO-*exo*, catalyzes the formation of the same *exo* cycloadduct as **13G5**, while *endo*-Diels–Alderase **7D4** from BCO-*endo* catalyzes the formation of the same *endo* adduct as **4D5**. Despite important differences in the structures of the haptens used to generate them, the racemic nature of the BCOs and achiral nature of the CPY and

Scheme 7. AM1 Calculations on the Base-Catalyzed Equilibrium between *endo*-14 and *exo*-14 Diels–Alder Adducts**Scheme 8.** Final Steps toward the Enantiomerically Pure *exo*-14 Adduct

CPQ haptens, all of the antibodies catalyze the formation of one *exo* and one *endo* adduct. Having established the absolute stereochemistries of the products from one set of antibodies,

we can conclude that antibody **22C8** catalyzes the formation of the *exo*- (3*S*,4*S*) adduct and **7D4** catalyzes the formation of the *endo*-(3*R*,4*S*) adduct.

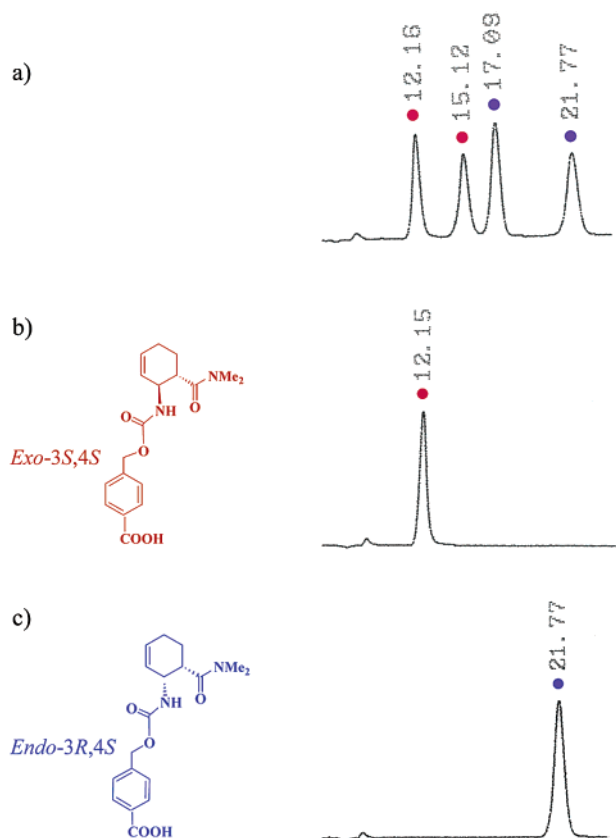


Figure 3. Determination of the absolute configuration of the antibody-catalyzed adducts.

Quantitative Determination of the Enantioselectivity of the *endo* Diels–Alderase **4D5 and the *exo* Diels–Alderase **13G5**.** Five buffered solutions (pH = 7.4, PBS) of **13G5** and three buffered solutions of **4D5** were prepared. The solutions each contained 20 μ M of the corresponding antibody, 8 mM of the diene, and 4 mM of the dienophile.

The antibody-catalyzed reactions were analyzed once a day, following the HPLC protocol described in the Supporting Information. The rate of formation of *exo* adduct produced in the reaction catalyzed by **13G5** ($R^2 = 0.97$) is constant (Figure 4a). Similar results were obtained for the reaction catalyzed by **4D5** ($R^2 = 0.99$, Figure 4b). The five background solutions were also analyzed and gave a good linearity ($R^2 = 0.96$ for the *exo* adducts in Figure 4a and $R^2 = 0.99$ for the *endo* adducts in Figure 4b). It is clear from the plotted data in Figure 4 that neither *exo*-Diels–Alderase **13G5** catalyzed the formation of any of the *endo* adducts, nor did *endo*-Diels–Alderase **4D5** catalyze the formation of any of the *exo* adducts.

Figure 5 shows a background trace **A** after 139.37 h (about 6 days) of reaction. The peaks at 12.05 and 15.01 min correspond to equal amounts of *exo*-(*S,S*) and *exo*-(*R,R*) adducts, respectively, and the peaks at 17.02 and 21.69 min correspond to equal amounts of *endo*-(*3S,4R*) and *endo*-(*3R,4S*) cycloadducts, respectively. Traces **B** and **C** correspond to **13G5**- and **4D5**-catalyzed reactions that were stopped and analyzed after approximately the same reaction time (165.77 and 167.07 h, respectively). In trace **B** the peak at 12.04 min is noticeably enlarged with respect to the peak for the enantiomer at 15.00 min, while the *endo* mixture remains racemic. Trace **C** shows

an increased peak at 21.73 min with respect to the peak for the enantiomer at 17.08 min, while the *exo* mixture remains racemic.

On the basis of the experimentally determined amounts of enantiomeric adducts in the antibody-catalyzed reactions, we calculated an % ee = $98 \pm 2\%$ ee for *exo* Diels–Alderase **13G5** and $90 \pm 2\%$ ee for *endo* Diels–Alderase **4D5**, after subtracting the amount of racemic adducts produced in the background reaction at the same time. The small, random fluctuations of the enantiomeric ratios observed on every single measurement are within experimental error, eliminating the possibility of product inhibition. A steady decrease of enantiomeric ratio with time would have been expected under product inhibition conditions. These enantiomeric excesses indicate that there are differences in free energies of activation of at least 2.7 and 1.8 kcal/mol, respectively, for formation of the major and minor enantiomers by **13G5** and **4D5**, respectively, at 37 $^{\circ}$ C.

Computational Explanations of the Origins of Enantioselective Catalysis. Methodology. Quantum mechanical calculations summarized in Figure 8 assessed the effect of hydrogen-bonding residues on the potential energy surface of the *exo* Diels–Alder reaction between methyl *N*-butadienyl carbamate (diene **15**) used as a model for diene **1**, and *N,N*-dimethylacrylamide shown in Figure 6.

All stationary points were optimized and characterized by frequency analysis at the B3LYP/6-31+G** level. The reported energies correspond to single-point calculations at the B3LYP³³/6-311+G** level on these B3LYP/6-31+G** geometries. The reported energies include zero-point energy corrections scaled by 0.9804.³⁴

Calculations on the transition states of the Diels–Alder reaction between diene **1** and *N,N*-dimethylacrylamide were then carried out to obtain a more realistic structure for the docking procedure (Figure 9). All stationary points for this larger system were fully optimized at the B3LYP/6-31G* level with zero-point energy corrections scaled by 0.9804.³³ Calculations were performed with Gaussian 98.³⁵

Docking of the enantiomeric *exo* transition states within the X-ray structure of *exo*-Diels–Alderase **13G5** was performed with Autodock V3.0³⁶ that allows a flexible ligand to interact with a rigid macromolecule.

All molecular dynamics simulations were performed with the AMBER 5.0 suite of programs³⁷ and the parm94 parameter set.³⁸ After flexible docking, the lowest-energy structure from the lowest-energy cluster of each competing enantiomeric *exo*

(34) Wong, M. W. *Chem. Phys. Lett.* **1996**, *256*, 391–399.

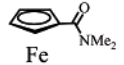
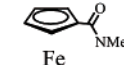
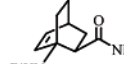

(35) Frisch, M. J.; Trucks, G. W.; Schlegel, H. B.; Scuseria, G. E.; Robb, M. A.; Cheeseman, J. R.; Zakrzewski, V. G.; Montgomery, J. A., Jr.; Stratmann, R. E.; Burant, J. C.; Dapprich, S.; Millam, J. M.; Daniels, A. D.; Kudin, K. N.; Strain, M. C.; Farkas, O.; Tomasi, J.; Barone, V.; Cossi, M.; Cammi, R.; Mennucci, B.; Pomelli, C.; Adamo, C.; Clifford, S.; Ochterski, J.; Petersson, G. A.; Ayala, P. Y.; Cui, Q.; Morokuma, K.; Malick, D. K.; Rabuck, A. D.; Raghavachari, K.; Foresman, J. B.; Cioslowski, J.; Ortiz, J. V.; Stefanov, B. B.; Liu, G.; Liashenko, A.; Piskorz, P.; Komaromi, I.; Gomperts, R.; Martin, R. L.; Fox, D. J.; Keith, T.; Al-Laham, M. A.; Peng, C. Y.; Nanayakkara, A.; Gonzalez, C.; Challacombe, M.; Gill, P. M. W.; Johnson, B. G.; Chen, W.; Wong, M. W.; Andres, J. L.; Head-Gordon, M.; Replogle, E. S.; Pople, J. A. *Gaussian 98*, revision A.7; Gaussian, Inc.: Pittsburgh, PA, 1998.

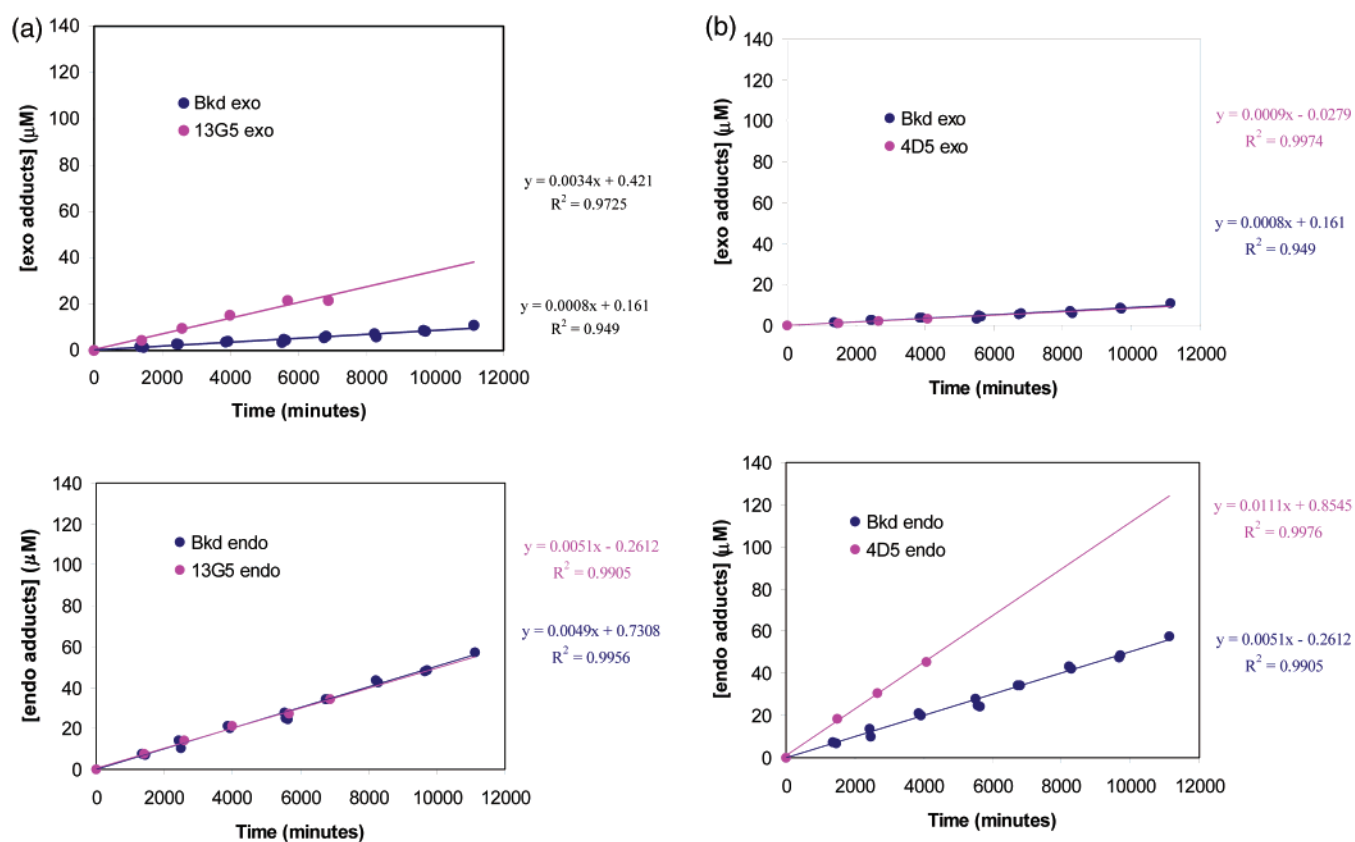
(36) Morris, G. M.; Goodsell, D. S.; Halliday, R. S.; Huey, R.; Hart, W. E.; Belew, R. K.; Olson, A. J. *J. Comput. Chem.* **1998**, *19*, 1639–1662.

(37) Pearlman, D. A.; Case, D. A.; Caldwell, J. W.; Ross, W. S.; Cheatham, T. E., III; DeBolt, S.; Ferguson, D.; Seibel, G.; Kollman, P. *Comput. Phys. Commun.* **1995**, *91*, 1–41.

(38) Cornell, W. D.; Cieplak, P.; Bayly, C. I.; Gould, I. R.; Merz, K. M., Jr.; Ferguson, D. M.; Spellmeyer, D. C.; Fox, T.; Caldwell, J. W.; Kollman, P. *J. Am. Chem. Soc.* **1995**, *117*, 5179–5197.

Table 1. Enantioselectivity of the Entire Pool of Catalytic Antibodies Elicited along with **13G5** and **4D5**; Filled Circles Represent the Main Stereoisomer Produced by Each Antibody

Hapten	Antibody	<i>Exo-3S,4S</i>	<i>Exo-3R,4R</i>	<i>Endo-3R,4S</i>	<i>Endo-3S,4R</i>
 CPY  CPQ	13G5	●			
	4D3	●			
	7G8	●			
	2A3	●			
	6D7	●			
	14D9	●			
	2A3				●
 BCO- <i>exo</i>  BCO- <i>endo</i>	4D5				●
	8G2				●
	12F10				●
	15C1				●
	9B4				●
	1F4				●
	12D2				●
	7D10	●			
	22C8	●			
	7D4				●

**Figure 4.** (a) **13G5** production of *exo* and *endo* adducts. (b) **4D5** production of *exo* and *endo* adducts.

transition state was selected as the initial system for the molecular dynamics simulations.

Quantum Mechanical Theozymes. Three key residues in the active site of antibody **13G5** appeared to be responsible for

the observed catalysis, as determined by X-ray crystallography studies of the *exo* Diels–Alderase inhibitor complex at 1.95 Å resolution (Figure 7).¹⁶ It was previously postulated that Tyr-L36 activates *N,N*-dimethylacrylamide for nucleophilic attack

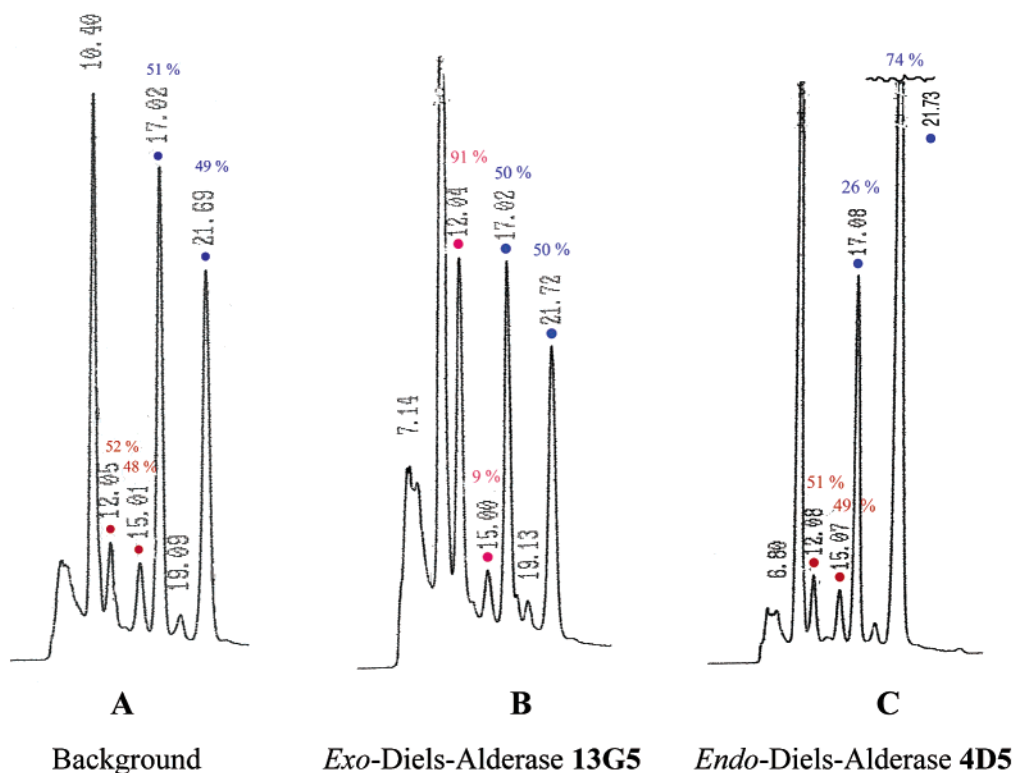


Figure 5. Chiral HPLC traces of Diels–Alder adducts produced by **13G5** and **4D5**.

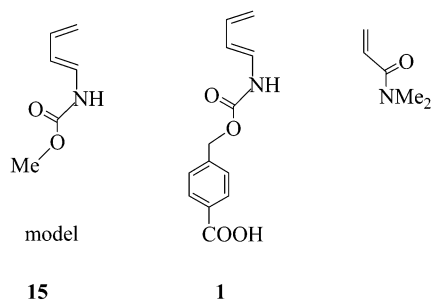


Figure 6. Dienes and dienophile used in the calculations.

by hydrogen bonding to the carbonyl group.¹⁶ Asparagine-L91 and aspartic acid-H50 hydrogen bond to the carboxylate side chain of the inhibitor that substitutes for the carbamate group of the diene **1** substrate. As stated earlier, the four possible ortho transition states, *endo* and *exo*, can be accommodated in the active site of **13G5**, but only the *exo* transition states maintained the hydrogen-bonding motif that accounts for inhibitor recognition.¹⁶ In this *exo* conformation, tyrosine-L36 still hydrogen bonds to the carbonyl of *N,N*-dimethylacrylamide, while aspartate-H50 forms a hydrogen bond with the carbamate NH, and asparagine-L91, with the carbamate carbonyl.

To test the ability of these residues to preferentially bind the *exo* transition state, a model system was studied. It consisted of *N,N*-dimethylacrylamide, methyl *N*-butadienyl carbamate as the diene, a formamide molecule to model the asparagine residue (Asn-L91), a water molecule for the tyrosine residue (Tyr-L36), and a formate molecule to mimic the aspartate residue (Asp-H50). The local minima corresponding to the hydrogen-bonding situations in the antibody were located. When formamide is hydrogen-bonded to the carbamate carbonyl, the energy of activation of the *exo* transition state (Figure 8b) increases by

0.5 kcal/mol with respect to the uncatalyzed reaction (Figure 8a) due to a preferential stabilization of the hydrogen-bonded reactant diene (−4.3 kcal/mol) over the transition state (−3.8 kcal/mol). This result is in agreement with the fact that electron-withdrawing groups increase the energy of activation of a normal³⁹ electron demand Diels–Alder reaction between an electron rich diene and electron-deficient dienophile.⁴⁰

A water molecule hydrogen-bonded to the dienophile carbonyl decreases the energy of activation of the *exo* transition state (Figure 8c) by 1.1 kcal/mol with respect to the uncatalyzed reaction, due to preferential stabilization of the transition state (−6.5 kcal/mol) over the hydrogen-bonded reactant dienophile (−5.4 kcal/mol).

The strongest accelerating effect occurs when a formate anion is hydrogen-bonded to the carbamate NH group (Figure 8d). The energy of activation of the *exo* transition state is decreased by 7.4 kcal/mol due to a preferential stabilization of the transition state (−29.0 kcal/mol) over the hydrogen-bonded reactant diene (−21.6 kcal/mol).

The asparagine residue probably does not catalyze the reaction, but rather deactivates the diene, although it may play a role during the initial molecular recognition event between the diene and antibody **13G5**. The tyrosine and aspartate residues do activate diene and dienophile toward the *exo* Diels–Alder reaction, through hydrogen bonding.

Calculations on the *exo* transition state catalyzed simultaneously by molecules of water and formate show that there is a synergistic stabilizing effect of 1.9 kcal/mol on the energy of activation. In this case, the energy of activation (Figure 8e) decreases by 10.4 kcal/mol with respect to the uncatalyzed reaction, due to a preferential stabilization of the transition state

(39) Sustmann, R. *Tetrahedron Lett.* **1971**, 2721–2724.

(40) Sustmann, R.; Shubert, R. *Angew. Chem., Int. Ed. Engl.* **1972**, *11*, 840.

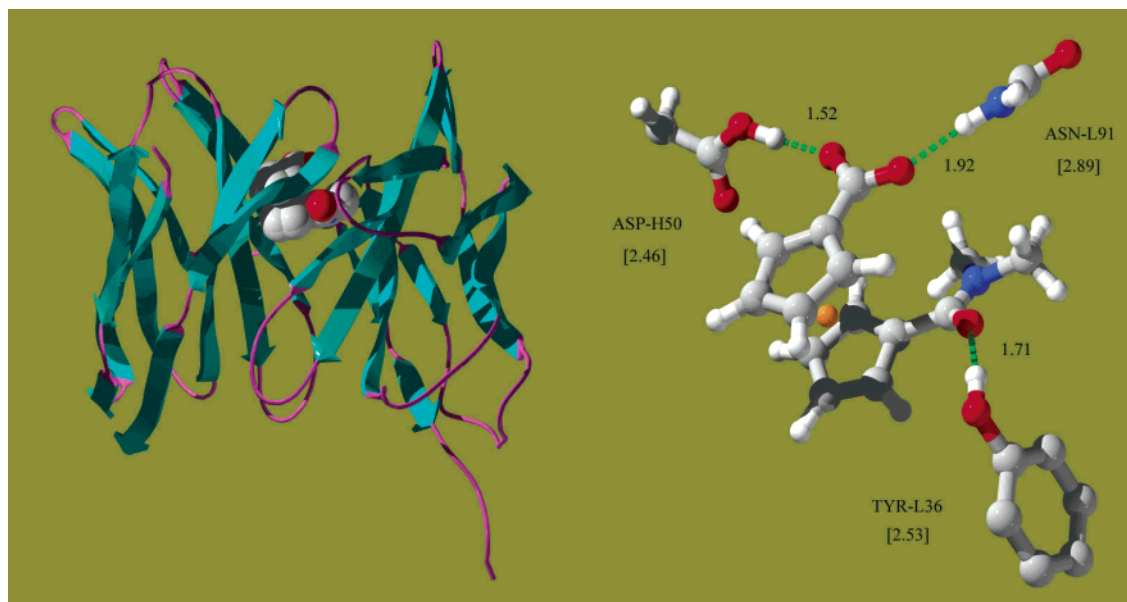


Figure 7. Exo Diels–Alderase **13G5** inhibitor complex at 1.95 resolution.

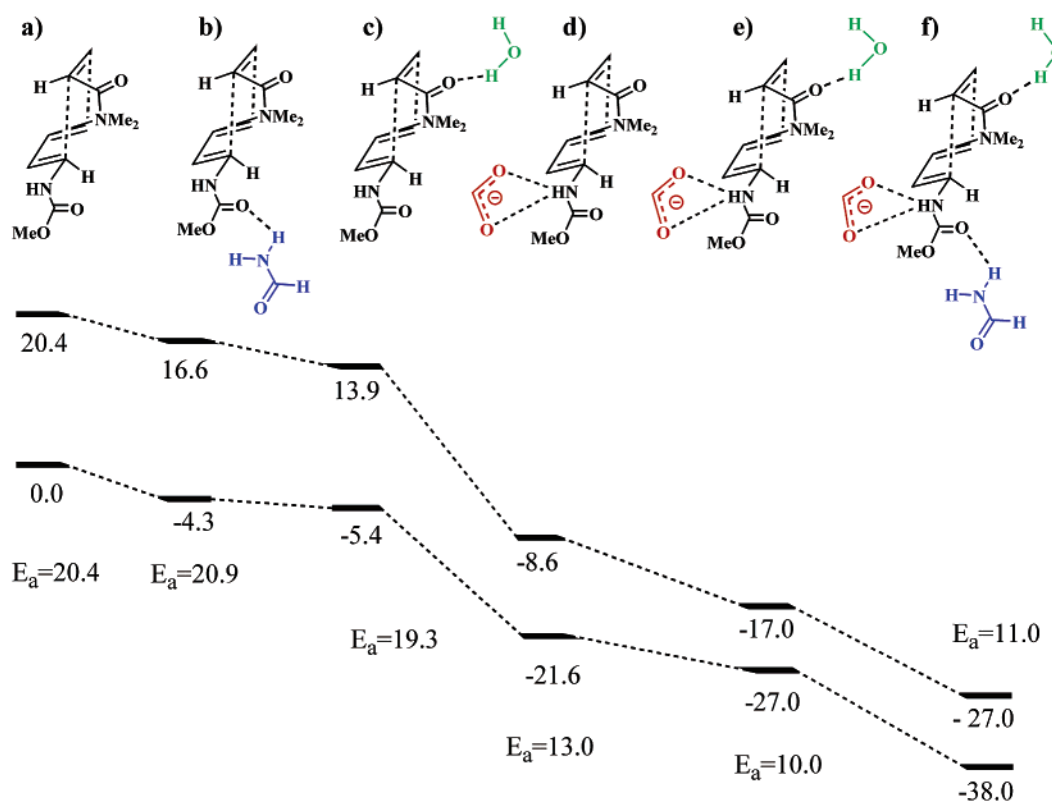


Figure 8. Relative energies of activation (E_a) in kcal/mol of the *exo* Diels–Alder reaction catalyzed by different arrangements of hydrogen-bonding groups. Higher bars correspond to the energies of the transition states shown (a–f), and lower bars represent the corresponding substrates, hydrogen-bonded to formamide, water or formate when required.

(−37.4 kcal/mol) over the corresponding hydrogen-bonded reactants (−27.0 kcal/mol). These two catalytic hydrogen-bonding interactions each cause asynchronicity and charge separation in the transition state. When both are present, the effects are cooperative, and the maximum charge separation is favored. The orthogonal orientation of Tyr-L36 and Asp-H50 within the active site of **13G5** permits maximum delocalization of charge in the *exo* transition state. Inclusion of the formamide molecule at this point increases the energy of activation by 1.0 kcal/mol (Figure 8f), showing that the deactivating effect of

the asparagine residue is enhanced in the presence of the catalytic residues.

The B3LYP/6-31+G** optimized geometries are substantially different from the HF/3-21G geometries of simplified models reported previously,^{12d} although the qualitative conclusions about activation energies are the same.

The effects of both catalytic residues on the conformation and relative energies of the *endo* and *exo* transition states between diene **1** and *N,N*-dimethylacrylamide were explored at the B3LYP/6-31G* level of theory.

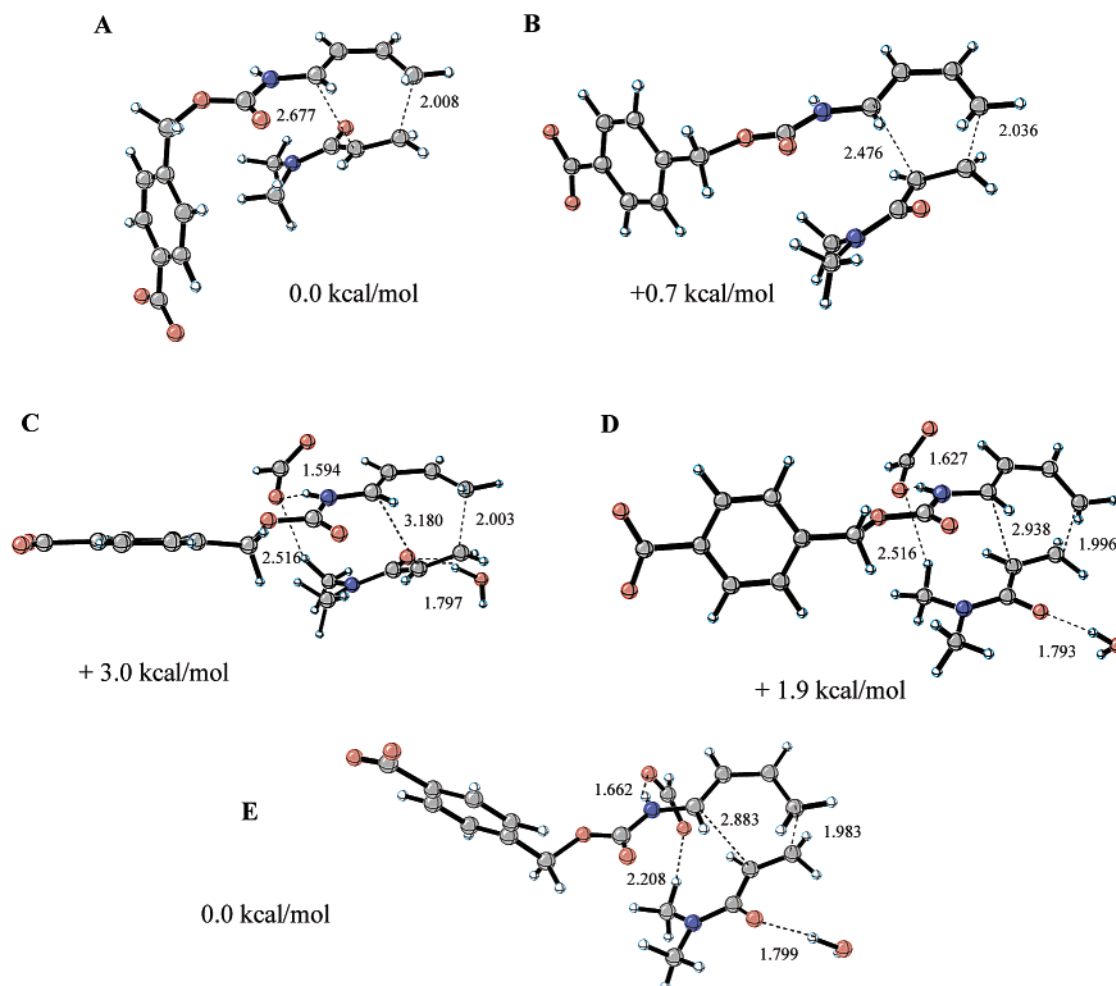


Figure 9. Effect of the catalytic groups on the diastereoselectivity of the Diels–Alder reaction.

The *endo* transition state (Figure 9A) is 0.7 kcal/mol more stable than the *exo* TS in the gas phase (Figure 9B), in agreement with the experimentally observed diastereoisomeric ratio of methyl ester derivatives obtained under kinetic control in refluxing toluene (66:34, 0.5 kcal/mol). The diastereoselectivity increases when the reaction is carried out in water at 37 °C (85:15, 1.0 kcal/mol).

When the formate anion hydrogen-bonds to the carbamate NH group and the water hydrogen-bonds to the dienophile carbonyl, the *exo* TS (Figure 9D) becomes 1.1 kcal/mol more stable than the *endo* TS (Figure 9C).

As noted earlier, the catalytic hydrogen-bonding interactions cause asynchronicity and charge separation in the transition state. The charge of the carbonyl oxygen of the dienophile changes from -0.58 (Figure 9, A or B) to -0.63 (Figure 9, C or D) after hydrogen-bonding to a water molecule. The charge on the formate oxygen hydrogen-bonded to the carbamate HN changes from -0.60 to -0.57 upon hydrogen-bonding. The switch in stereoselectivity observed upon hydrogen-bond formation to these two catalytic groups could be a consequence of the increased negative charge on these two oxygens and their mutual electrostatic repulsion in the *endo* TS (Figure 9C). In the *exo* transition states (Figure 9, D and E) this electrostatic repulsion is minimized because the two oxygens are separated from each other. Antibody **13G5** has aspartate and tyrosine residues in

close contact with the inhibitor in the active site and is an *exo* Diels–Alderase.

Docking Studies. Docking of the lowest-energy *exo*-(*R,R*) transition state, shown in Figure 9E, and its mirror image *exo*-(*S,S*) were carried out.

HF/6-31G charges were fitted to the electrostatic potential of these quantum mechanically obtained transition states, according to the Merz–Singh–Kollman scheme. The transition states were manually predocked into **13G5** using the Insight II/Discover software package.⁴² The values of the charges induced on the water molecule by the reacting dienophile were used to manually modify the charges in the side-chain atoms of the Tyr-L36 that the water mimicks. Likewise, charges developed on the formate molecule by the reacting diene were translated onto the Asp-H50 residue. These changes were performed under the assumption that the two hydrogen bonds, one to Asp-H50 and the second to Tyr-L36, are crucial for enantioselection and catalysis.

Autodock V3.0 utilizes a genetic algorithm technique to sample potential binding modes. This Lamarckian genetic algorithm was used to search the conformational space of the TS within the active site. It calculates the interaction energy

(41) Vargas, R.; Garza, J.; Dixon, D. A.; Hay, B. P. *J. Am. Chem. Soc.* **2000**, *122*, 4750–4755.

(42) InsightII/Discover; Biosym/Molecular Simulations Inc.: San Diego, CA.

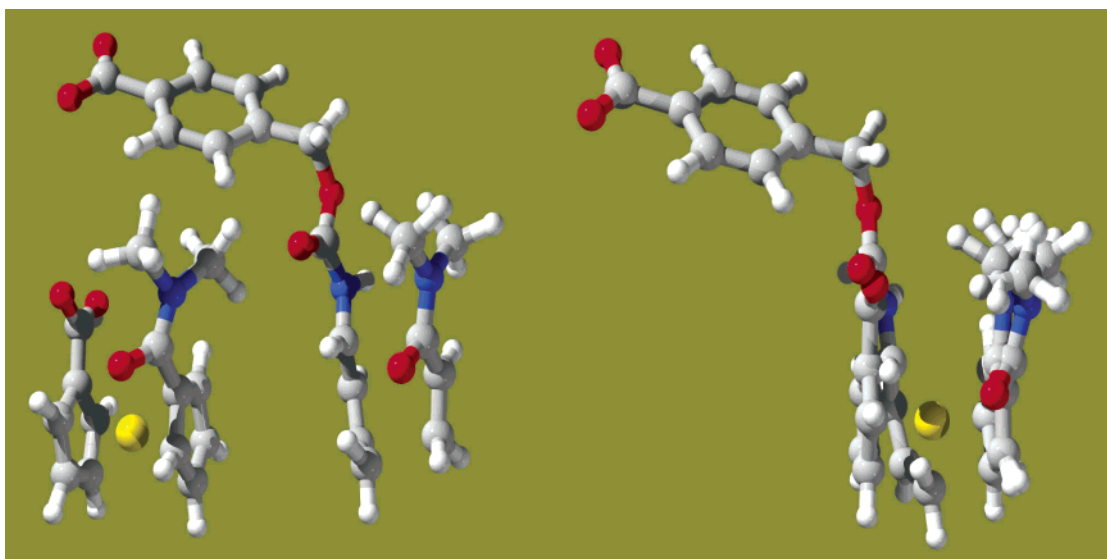


Figure 10. Inhibitor bound to *exo* Diels–Alderase **13G5** (left) and the *exo*-(*S,S*) transition state, (Figure 9E), middle. They are superimposed on the right.

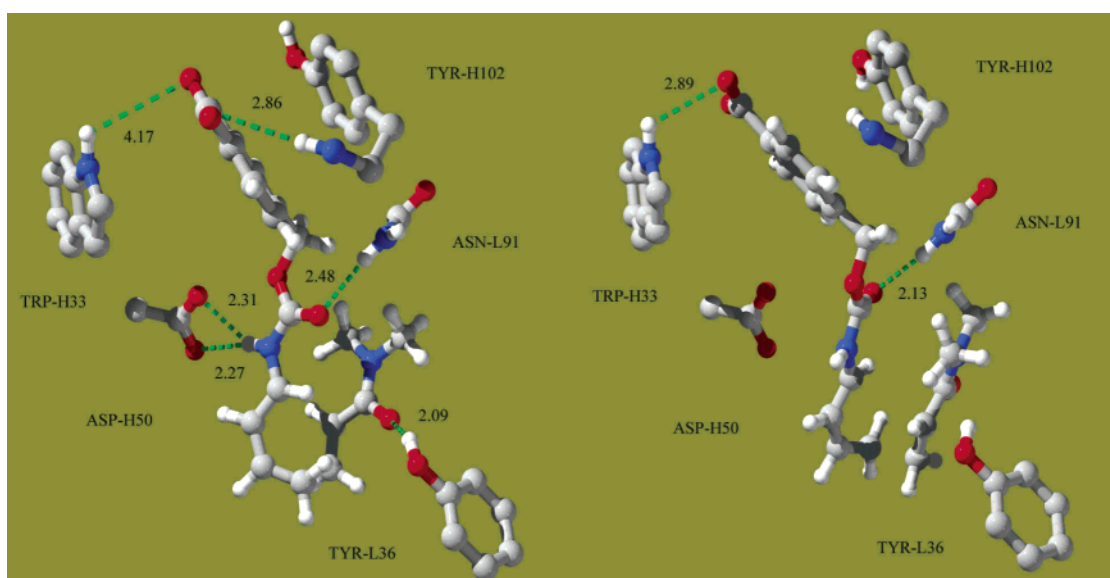


Figure 11. Rigid transition-state docking. The *exo*-(*S,S*)-TS is on the left, and the *exo*-(*R,R*)-TS is on the right.

utilizing grid-based affinity potentials to describe the protein. Interaction energies produced by Autodock V3.0 have been parametrized to reproduce experimental free energies of binding from aqueous solution.³⁵

Two different docking simulations were performed with both enantiomeric *exo* transition states. The first strategy involved docking the frozen transition states, *exo*-(*R,R*) and *exo*-(*S,S*), within the rigid framework of antibody **13G5**. Figure 10 shows the structure of the inhibitor bound in the crystal structure of **13G5** on the left, and the computed *exo*-(*S,S*) transition state (enantiomer of figure 9E) with the water and formate molecules removed in the middle. The superimposed structures on the right of Figure 10 show that the three hydrogen-bonding groups, namely the carbonyls of the diene and dienophile and the NH group of the diene carbamate, occupy almost identical regions of space. This observation strongly suggests that the experimentally catalyzed *exo*-(*S,S*) transition state fits nicely in the active site, while the enantiomeric *exo*-(*R,R*) transition state does not.

The second strategy involved docking the flexible transition states into the rigid active site of antibody **13G5**, followed by molecular dynamics relaxation of the hydrated antibody around the bound and frozen transition state. This latter approach was designed to study the effect of the conformational flexibility of the diene in the recognition event during the docking simulation and to address the role of induced-fit on binding.

Docking the frozen transition states within the rigid framework of antibody **13G5** resulted in only one conformational cluster for the *exo*-(*S,S*) transition state and two clusters for the *exo*-(*R,R*). The mean docked energy of the *exo*-(*S,S*) cluster is -12.5 kcal/mol. The mean docked energy of the lowest-energy *exo*-(*R,R*) cluster containing 118 out of 120 total runs is -11.1 kcal/mol. The corresponding docked structures are shown in Figure 11. When no conformational changes are allowed in either the TS or the antibody, the experimentally observed *exo*-(*S,S*) TS fits perfectly in the active site of Ab **13G5** in a productive orientation that preserves the three hydrogen bonds responsible for inhibitor recognition. A closer look at the active

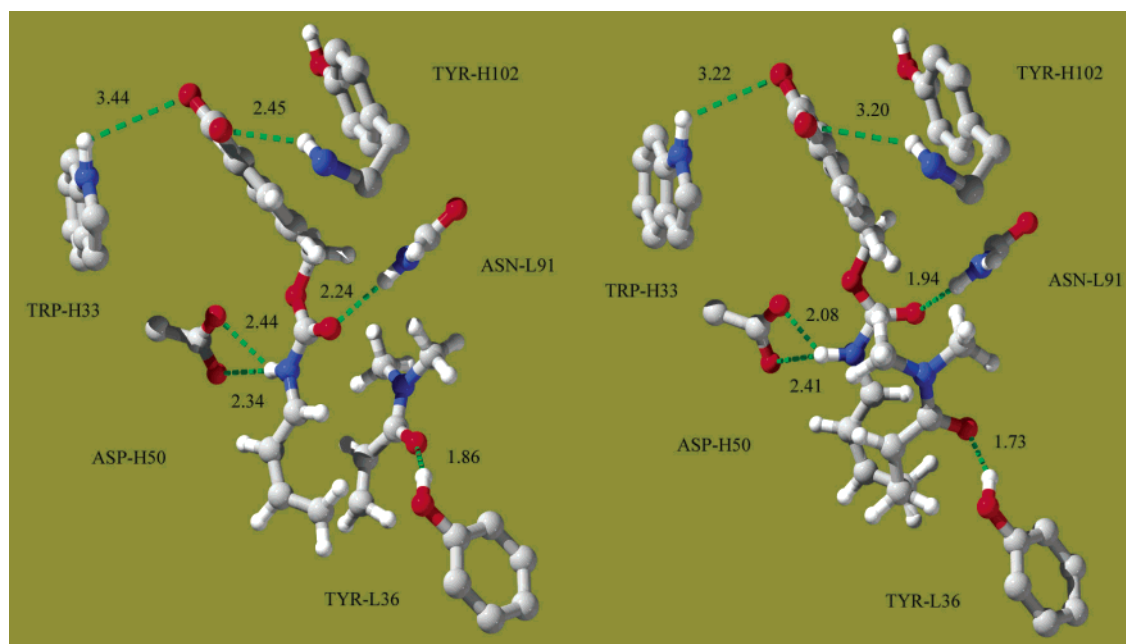


Figure 12. Flexible transition-state docking. The *exo*-(*S,S*)-TS is on the left, and the *exo*-(*R,R*)-TS is on the right.

site reveals that both oxygens of the Asp-50 carboxylate are hydrogen-bonded to the carbamate NH with distances of 2.31 and 2.27 Å. Asn-91 is hydrogen-bonded to the carbamate carbonyl (3.01 Å), and Tyr-36 forms a hydrogen bond to the dienophile carbonyl (2.09 Å). The electron-poor benzoate group of the diene is π -stacked between the two electron-rich aromatic residues of Tryptophan-H33 (Trp-H33) and Tyr-H102 with interring distances between 3 and 4 Å. The backbone NH of Tyr-H102 constitutes the fourth point of recognition by weakly hydrogen-bonding the benzoate oxygen (2.86 Å).

On the contrary, the *exo*-(*R,R*) TS does not dock in a productive orientation. In the lowest-energy complex shown in Figure 11, the benzoate group of the Diels–Alder TS is placed between the two aromatic residues, Trp-H33 and Tyr-H102, in the same orientation as the *exo*-(*S,S*) TS. Nevertheless, the transition state as a whole has to rotate to preserve the conformation of the diene chain. This rotation places the carbamate NH and the dienophile carbonyl perpendicular to the polar residues Asp-H50 and Tyr-L36, preventing the formation of catalytic hydrogen bonds. Only one hydrogen bond between Asn-L91 and the carbamate carbonyl is formed.

These results suggest that the mature *exo*-Diels–Alderase **13G5** is capable of binding the experimentally observed *exo*-(*S,S*) TS without undergoing important changes in its quaternary structure. Essentially a lock-and-key mechanism^{43,44} explains the enantioselectivity in this case.

Flexible docking studies were also carried out to assess the role of transition-state flexibility on docking. Only rotations about bonds with relatively low barriers need to be included in such calculations (<4 kcal/mol). The barriers of rotation around the N–CO of amides⁴⁵ are about 17–18 kcal/mol, increasing up to 20 kcal/mol as the dielectric constant and hydrogen-bond donating ability of the solvent increase,⁴⁶ and decrease to 15–17 kcal/mol⁴⁷ in carbamates becoming insensitive to solvent polarity. Rotational barriers around the O–CO bond of carbamates are about 16 kcal/mol,⁴⁸ decreasing to 10 kcal/mol⁴⁹ in methyl esters. Rotational barriers of around 6 kcal/mol have

been calculated for the rotation of a carboxylate out of the plane of a phenyl ring.⁵⁰

Rotation around the OCO–CH₂R bond of esters necessitates rotational barriers only from 0.6 to 1.4 kcal/mol,⁵¹ and rotational barriers of the Ph–CH₂X bond require 1–1.6 kcal/mol.⁵² During the flexible docking procedure, only the dihedral angles around the C–O and the O–Ph bonds of the diene were allowed to change to avoid the appearance of unrealistic conformations.

Two conformational clusters for each transition state were obtained; the lowest in energy containing most of the structures in both cases. The left side of Figure 12 shows the lowest-energy conformer of the (*S,S*) transition state docked into Ab **13G5**. The mean docked energy of the lowest-energy cluster containing 118 out of 120 total runs, is –13.1 kcal/mol; this value also corresponds to the energy of the lowest-energy conformer within the cluster. The right side of Figure 12 shows the lowest-energy conformer of the *exo*-(*R,R*) transition state docked into Ab **13G5**. The average docked energy of the lowest-energy cluster containing 119 out of 120 total runs is –13.0 kcal/mol and also corresponds to the energy of the lowest conformer within the cluster. There is now no preference for the *exo*-(*S,S*) transition state leading to the experimentally observed enantiomerically

- (43) Wedemayer, G. J.; Patten, P. A.; Wang, L. H.; Schultz, P. G.; Stevens, R. C. *Science* **1997**, *276*, 1665–1669.
- (44) Amit, A. G.; Mariuzza, R. A.; Phillips, S. E. V.; Poljak, R. J. *Science* **1986**, *233*, 747.
- (45) For reviews, see: (a) Stewart, W. E.; Siddall, T. H., III. *Chem. Rev.* **1970**, *70*, 517. (b) Oki, M. *Applications of Dynamic NMR Spectroscopy to Organic Chemistry*; VCH: Deerfield Beach, 1985; Chapter 2.
- (46) (a) Drakenberg, T.; Dahlqvist, K.-I.; Forsen, S. *J. Phys. Chem.* **1972**, *76*, 2178–2183. (b) Eberhardt, E. S.; Loh, S. N.; Hinck, A. P.; Raines, R. T. *J. Am. Chem. Soc.* **1992**, *114*, 5437–5439.
- (47) Cox, C.; Lectka, T. *J. Org. Chem.* **1998**, *63*, 2426–2427.
- (48) Van der Werf, S.; Olijnsma, T.; Engberts, J. B. F. N. *Tetrahedron Lett.* **1967**, 689–693.
- (49) (a) Review: Jone, G. I. L.; Owen, N. L. *J. Mol. Struct.* **1973**, *18*, 1. (b) Grindley, T. B. *Tetrahedron Lett.* **1982**, *23*, 1757–1760.
- (50) Nelson, M. R.; Borkman, R. F. *J. Mol. Struct. (THEOCHEM)* **1998**, *432*, 247–255.
- (51) Karabatsos, G. J.; His, N.; Orzech, C. E., Jr. *Tetrahedron Lett.* **1966**, 4639–4643.
- (52) (a) Abraham, R. J.; Bakke, J. M. *Tetrahedron* **1978**, *34*, 2947–2951. (b) Mons, M.; Robertson, E. G.; Simons, J. P. *J. Phys. Chem. A* **2000**, *104*, 1430–1437.

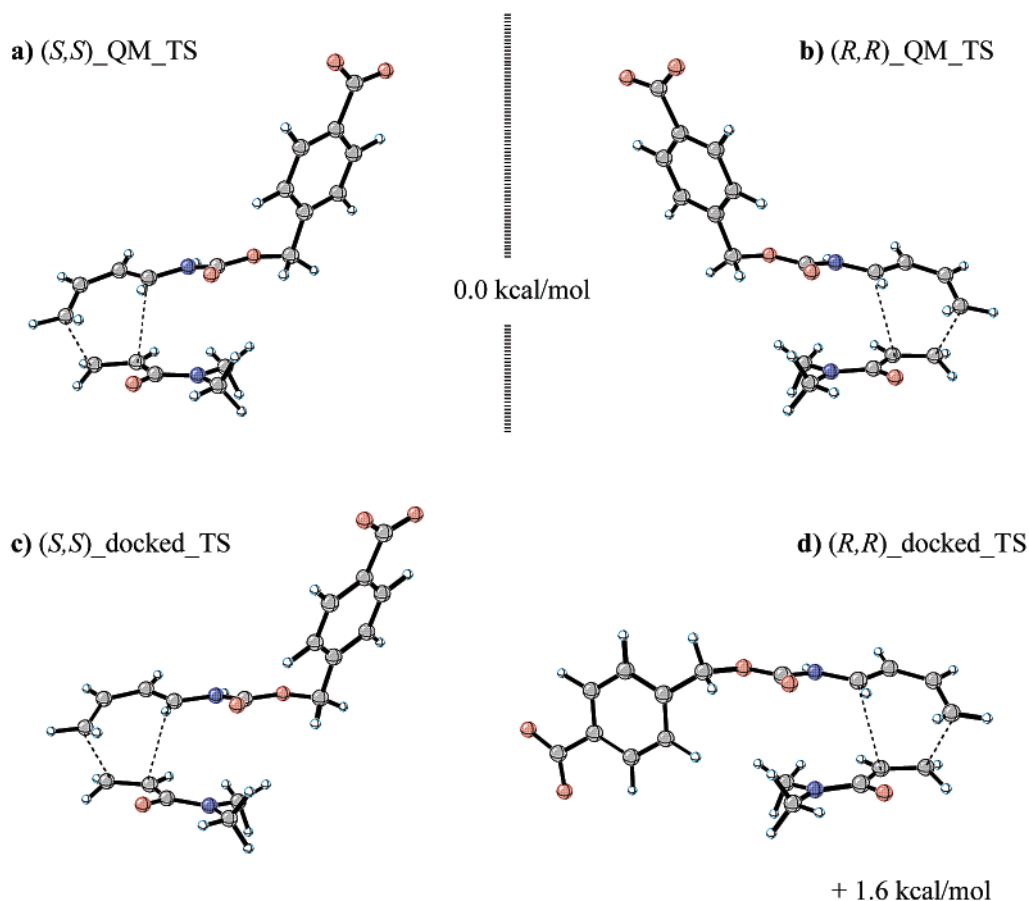


Figure 13. Conformational changes on the enantiomeric transition states upon flexible docking. The *exo*-(*S,S*)-TS is on the left, and the *exo*-(*R,R*)-TS is on the right.

pure product. Both transition states are oriented within the active site in a fashion very similar to that of the rigidly docked *exo*-(*S,S*) transition state in Figure 11. The catalytic tyrosine residue (Tyr-L36) is hydrogen-bonded to the dienophile carbonyl, with a hydrogen-bond length of 1.86 Å in the *exo*-(*S,S*) TS and 1.73 Å in the *exo*-(*R,R*) TS. Both oxygen atoms of the catalytic aspartate residue (Asp-H50) are hydrogen-bonded to the diene NH. The bond lengths are 2.34 and 2.44 Å in the *exo*-(*S,S*) TS and 2.08 and 2.41 Å in the *exo*-(*R,R*) TS. Asn-L91 forms a hydrogen bond with the carbamate carbonyl that is slightly longer in the *exo*-(*S,S*) TS (2.24 Å) than in the *exo*-(*R,R*) TS (1.94 Å). In both cases, the fourth contact required for enantiodifferentiation⁵³ is obtained by a hydrogen bond between the backbone NH of Tyr-H102 and the benzoate oxygen.

The rigid and flexible docking of the *exo*-(*S,S*) TS gives rise to the same binding mode with very close hydrogen-bonding distances. Therefore, allowing conformational changes during the docking simulation does not improve the binding of *exo*-(*S,S*) TS. On the other hand, for the *exo*-(*R,R*) TS to fit in a productive orientation within the active site, a conformational change of the diene chain is necessary. To assess the energetic cost of this conformational change, single-point energy evaluations at the B3LYP/6-31G* level of theory were performed on the *exo*-(*R,R*) TS after the rigid and the flexible docking. The new conformation obtained after flexible docking is 1.6 kcal/mol higher in energy than the original transition-state

structure. Parts a and b of Figure 13 show the calculated structures of the enantiomeric transition states as mirror images of each other. Parts c and d of Figure 13 are the corresponding structures after flexible docking. Both the rigid and flexible docking studies show that the *exo*-(*S,S*) TS fits better in the active site.

Molecular Dynamics Studies

After flexible docking, antibody **13G5** was allowed to relax around the constrained docked structures of both transition states. In each case, 1000 steps of energy minimization were followed by a 280-ps molecular dynamics simulation of the antibody around the frozen transition states. The *exo*-(*S,S*) and *exo*-(*R,R*) structures in the protein were capped with a sphere of explicit water molecules centered at the transition structure with a radius of 20 Å. A Na⁺ counterion was added to neutralize the carboxylate of the diene. The sodium ion was positioned using the “addions” functionality of *xleap*, which defines an electrostatic grid and places the ion at the most negative point on that grid. In both cases, the ion was at least 22 Å distant from the closest atom in the docked transition states. The nonbonded cutoff for the van der Waals and electrostatic interactions occurred at 14 Å. All the protein residues and the water molecules were allowed to move (i.e., included in the “belly” option of AMBER) while the transition states remained frozen. A constant dielectric function was used that mimics the presence of water around the system when explicit water molecules are present.

(53) Mesecar, A. D.; Koshland, D. E., Jr. *Nature* **2000**, *403*, 614–615.

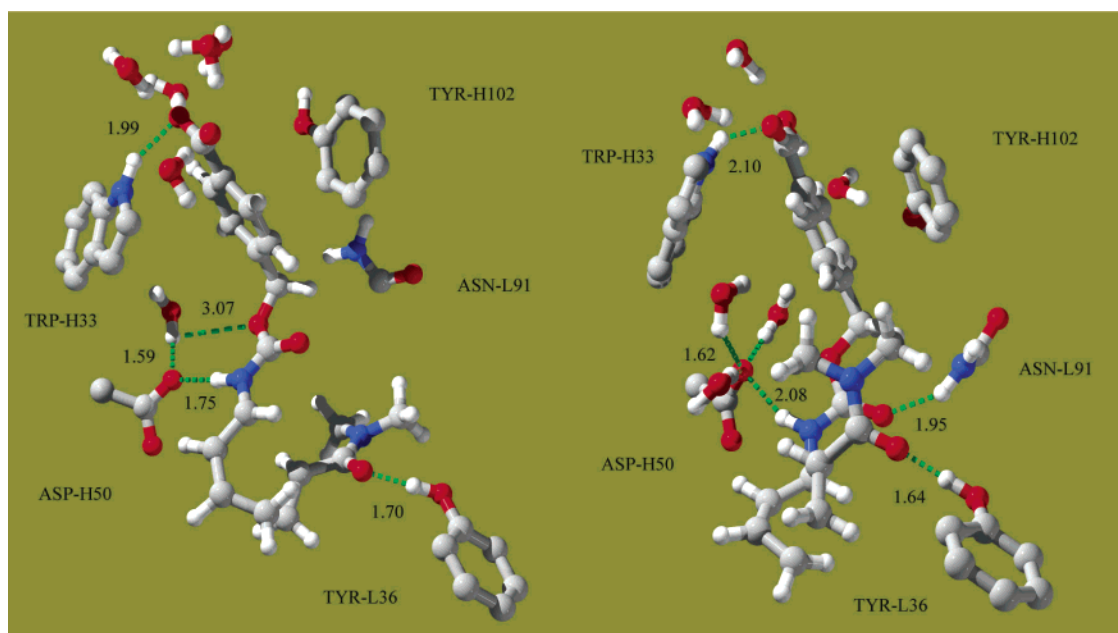


Figure 14. Molecular dynamics relaxation of *exo*-Diels–Alderase **13G5** around the flexibly docked transition states. The *exo*-(*S,S*)-TS is on the left, and the *exo*-(*R,R*)-TS is on the right.

During the initial minimization performed to remove bad contacts in the X-ray structure of **13G5**, distance constraints were introduced in the docked transition states among the carbon and hydrogen atoms of the reacting parts of the diene and dienophile, using the “NMR constraints” functionality of the SANDER module. This procedure ensured that the core of the transition state remained structurally as obtained quantum mechanically, allowing changes of the bond lengths of only ± 0.003 Å. Minimizations were run with a combination of 10 cycles of steepest descent, followed by 990 steps of the full conjugate gradient method without any constraints on protein bond lengths. After the initial minimization, heating and equilibration of the system were carried out for a total of 80 ps. Equilibration was assessed by monitoring temperature and total and potential energies versus time. A productive run of 200 ps was carried out, and 400 coordinates were saved for analysis. The dynamics were run with constraints on all bonds using the SHAKE⁵⁴ algorithm, and a time step of 1 fs. The average value of the temperature was maintained at the experimental temperature of 310 K, by means of the Berendsen coupling algorithm.⁵⁵

Visual inspection of the trajectories obtained for both (*S,S*) and (*R,R*) transition states revealed two important changes when compared to the initial structures originated during the flexible docking procedure. First, after the equilibration period, only one water molecule entered the active site when the *exo*-(*S,S*) TS was bound as a consequence of a tighter fitting between this TS and antibody **13G5** (Figure 14). This water molecule is strongly hydrogen-bonded to Asp-H50 (1.59 Å) and regularly forms a second hydrogen bond with the alkoxide oxygen of the carbamate. Asp-H50 moves closer to the carbamate NH (1.75 Å), strengthening this important catalytic interaction. By contrast, three water molecules entered the active site when *exo*-(*R,R*) TS was bound. They formed three strong hydrogen bonds

with the catalytic Asp-H50 with bond lengths that vary from 1.59 to 1.64 Å. These interactions decrease the electron density on the catalytic residue and keep it at 2.08 Å from the transition state, weakening the catalytic hydrogen bond between Asp-H50 and the carbamate HN.

Second, the decelerating interaction between Asp-L91 and the carbamate carbonyl is completely lost when the experimentally observed *exo*-(*S,S*) TS is bound, but it remains when the *exo*-(*R,R*) TS is bound. Catalytic residue Tyr-L36 reorients and hydrogen bonds the dienophile carbonyl *trans* to the C=C with shorter bond lengths (1.70 Å for *exo*-(*S,S*) TS and 1.64 Å for the *exo*-(*R,R*)).

These observations suggest that when the diene is recognized by Asp-H50 and Trp-H33 of the heavy chain, the *si* face is exposed, and the incoming dienophile can approach the diene from the back, presenting its *si* face to give the experimentally observed (*S,S*) product. When the diene is recognized simultaneously by the heavy (Asp-H50 and Trp-H33) and the light (Asn-L91) chains, the *re* face is exposed, and the dienophile can only approach the diene from the front, presenting its *re* face. This last arrangement is disfavored for three reasons: (1) It requires a conformational change of the *exo*-(*R,R*) transition state to fit the active site in a productive manner, with an energetic cost of 1.6 kcal/mol, (2) the most important electrostatic interaction from the catalytic point of view between Asp-H50 and the carbamate NH is weakened by solvation, and (3) the unfavorable hydrogen bond between Asp-L91 and the carbamate carbonyl, that disfavors binding of the transition state relative to the ground state, is still present.

Discussion

Hapten **CPY** can rotate freely around its axis to give a mixture of rotamers in solution. The functional arrangement in these rotamers corresponds to a racemic mixture of *endo* and *exo* Diels–Alder TS analogues. In principle, this hapten could be bound in a suitable conformation mimicking any of these four stereoisomeric transition states. Our experimental results show

(54) Ryckaert, J. P.; Ciccotti, G.; Berendsen, H. J. C. *J. Comput. Phys.* **1997**, *23*, 327–341.

(55) Berendsen, H. J. C.; Postma, J. P. M.; van Gunsteren, W. F.; DiNola, A.; Haak, J. R. *J. Chem. Phys.* **1984**, *81*, 3684.

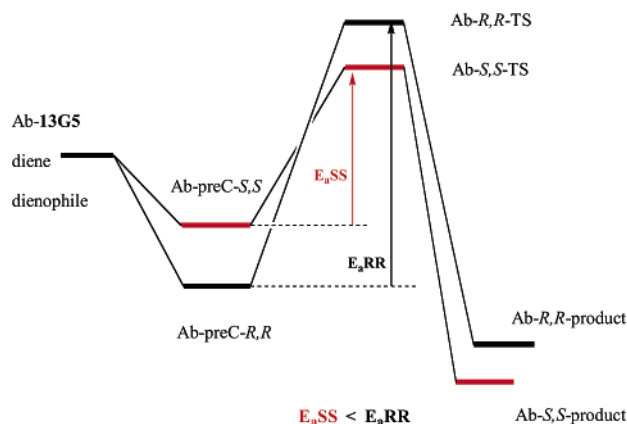


Figure 15. Postulated energy profile of the Diels–Alder reaction catalyzed by 13G5.

that antibody 13G5 catalyzes the formation of the *exo*-(*S,S*) adduct, and Table 1 indicates that all *exo*-Diels–Alderases elicited with hapten CPY also catalyze the formation of the same enantiomer. X-ray crystallography and computational studies suggested that Tyr-L36 and Asp-H50 catalyze the reaction by activating the dienophile and the diene, respectively. Asn-L91, on the other hand, increases the energy of activation of the reaction. Docking and molecular dynamics simulations showed that this latter deactivating interaction is lost when antibody 13G5 relaxes around the *exo*-(*S,S*) TS and remains when antibody 13G5 relaxes around the *exo*-(*R,R*) TS. Furthermore, the tighter fitting of the *exo*-(*S,S*) TS impedes solvation of the active site, maximizing the stabilizing interactions between the *exo*-(*S,S*) TS and the catalytic Tyr-L36 and Asp-H50 residues. It is reasonable to assume that the diene and dienophile form a van der Waals complex within the antibody-combining site in an orientation similar to that of the corresponding transition state before reacting. Although antibody 13G5 might be capable of stabilizing the *exo*-(*R,R*) complex to a greater extent than the enantiomeric *exo*-(*S,S*) complex, the *exo*-(*S,S*) TS is preferentially stabilized over the *exo*-(*R,R*) TS, giving rise to the (*S,S*) cycloadduct. (Figure 15)

This analysis correlates with an earlier observation on the enantioselectivity of antibody 14D9. This antibody catalyzes the transformation of achiral enol ethers into the corresponding (*S*) ketals despite preferential binding of the (*R*) intermediate.⁵⁶

The surprising consistency of the whole panel of antibodies obtained from the ferrocene hapten CPY raises a number of important questions about the origins of this stereoselectivity. First, why are only catalysts that induce one type of chirality in the product obtained from racemic haptens? One explanation is that all evolved from a single germline. If this were true, then all antibodies would be expected to have a high degree of conserved residues and probably to present a very similar spatial arrangement of catalytic groups. Clearly, it would be interesting to obtain all sequence data to analyze this possibility in detail.

Alternatively, if the panel of catalytic antibodies came from different germlines, it could be that they preferentially catalyze the formation of the *exo*-(*S,S*) TS because the immune system possesses an inherent bias toward one chirality due to the fact that all antibodies are formed from L-amino acids. It is well-known that proteases can only hydrolyze peptidic bonds between

two L residues, and this fact has recently been applied toward the design and synthesis of a potent and selective protease-resistant antibacterial agent variety of D-polypeptides.⁵⁷

In 1969 Jencks introduced the idea⁵⁸ that catalytic antibodies elicited in response to transition-state mimics might catalyze reactions by selective stabilization of the transition state more than the corresponding reactants, in analogy to enzymes. Many catalytic antibodies catalyze the hydrolysis of ester and amide bonds, or the formation of ester and amide bonds where one of the reactants is an amino acid of known stereochemistry, and other related reactions such as transesterification and ester aminolysis. Therefore, we could in principle determine whether the immune system possesses an inherent bias toward one chirality by analyzing the absolute stereochemistry of the products formed by antibodies elicited by racemic haptens. If the immune system were biased, all antibodies generated from racemic haptens would be expected to catalyze the formation of the same enantiomer of the product in a particular reaction.

Although no chiral centers are created during these processes, antibodies elicited by racemic peptide-like haptens have been shown to selectively react with only one enantiomer of the substrate.^{59–61} The absolute stereochemistry of the products was either (*R*)^{26,27} or (*S*).²⁸ In some cases the enantioselective discrimination was achieved by preferential binding of the substrate with the same chirality observed in the product.²⁶ In other cases, one enantiomer of the product was formed preferentially, despite the higher affinity of the antibody for other enantiomer of the hapten.²⁷

The observations suggest that, in principle, there is no innate reason the immune system would select a particular stereochemistry. Antibody 13G5 catalyzes the Diels–Alder reaction between a diene bearing a carbamate group and a dienophile with a dimethylamide moiety. This highly enantioselective reaction could be regarded as the formation of a β -dipeptide where two new stereocenters are created. Therefore, antibodies that catalyze the formation of the other two diastereoisomeric transition states of the Diels–Alder reaction, (*R,R*) and (*S,R*), should have been expected. The fact that no antibodies capable of catalyzing the formation of the (*R,R*) adduct were detected along with 13G5, despite the low concentration of hapten used during the immunization,⁶² could be explained by the fact that they all evolved from the same germ line or, alternatively, by the fact that antibodies were selected for binding to the TS analogue, TSA, and then for catalysis. The hapten used for

(57) Gill, T. J., III; Kunz, H. W.; Papermaster, D. S. *J. Biol. Chem.* **1967**, *242*, 3308.

(58) Jenks, W. P. *Catalysis in Chemistry and Immunology*; McGraw-Hill: New York, 1969; p 288.

(59) (a) Janda, K. D.; Benkovic, S. J.; Lerner, R. A. *Science* **1989**, *244*, 437–440. (b) Nakatani, T.; Hiratake, J.; Shinzaki, A.; Umeshita, R.; Suzuki, T.; Nishioka, T.; Nakajima, H.; Oda, J. *Tetrahedron Lett.* **1993**, *34*, 4945–4948. (c) Tanaka, F.; Kinoshita, K.; Tanimura, R.; Fujii, I. *J. Am. Chem. Soc.* **1996**, *118*, 2332–2339.

(60) (a) Cochran, A. G. *J. Am. Chem. Soc.* **1991**, *113*, 6670–6672. (b) Martin, M. T.; Angeles, T. S.; Sugawara, R.; Aman, N. I.; Napper, A. D.; Darsley, M. J.; Sanchez, R. I.; Booth, P.; Titmas, R. C. *J. Am. Chem. Soc.* **1994**, *116*, 6508–6512.

(61) (a) Guo, J.; Huang, W.; Scanlan, T. S. *J. Am. Chem. Soc.* **1994**, *116*, 6062–6069. (b) Lo, C.-H. L.; Wentworth, P.; Jung, K. W.; Yoon, J.; Ashley, J. A.; Janda, K. D. *J. Am. Chem. Soc.* **1997**, *119*, 10251–10252.

(62) For both the CPY and CPQ immunizations, 100 μ g (of a 5 mg/mL KLH conjugate) per mouse per injection were used. Four mice were immunized each with 100 μ g CPY–KLH (or CPQ–KLH) in 200 μ L RIBI adjuvant intraperitoneally. Two weeks later the mice were boosted again with another 100 μ g. The mice were bled 1 week later, and the titers were determined by ELISA. After 1 month, a final injection with 50 μ g of hapten–KLH in 100 μ L PBS was performed intravenously in the tail vein. Three days later the spleen was removed for fusion.

(56) Shabat, D.; Shulman, H.; Itzhaky, H.; Reymond, J.-L.; Keinan, E. *J. Chem. Soc., Chem. Commun.* **1998**, *16*, 1759–1760.

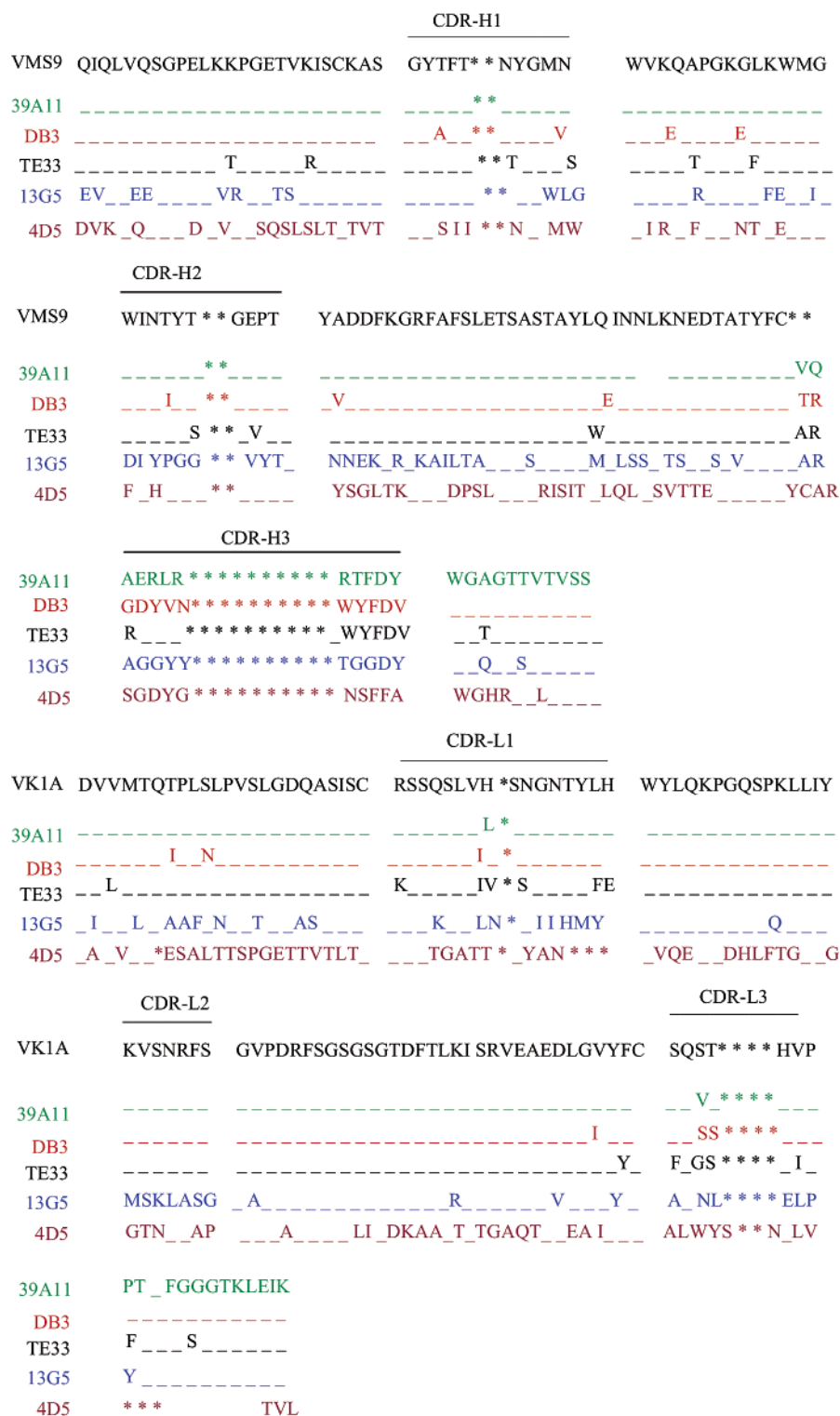


Figure 16. Sequences of the germ-line precursors, VMS9 and V_k1a, of the V_H and V_L regions of structurally related antibodies 39-A11, DB3, and TE33. The first two sequences correspond to antibodies 13G5 and 4D5 elicited toward a racemic TSA of a Diels–Alder reaction, very similar to the hapten used to generate the other Diels–Alderase 39-A11. Dashes indicate identical residues, and stars correspond to gaps in the sequences.

screening antibodies for binding to the TS analogue resembles the van der Waals complex between the reactants more closely than the transition state because the distance between the cyclopentadienyl rings in the ferrocene hapten is longer than the distances of the forming bonds in the transition state. Screening for binding would select antibodies that bind preferentially the rotamer of the hapten that mimics the (*R,R*) TS

analogue as depicted in the energetic profile shown in Figure 15. Considering that this (*R,R*) TS analogue would resemble a dipeptide made from D-amino acids, this postulate is in agreement with the experimental observation that D-polypeptides are more antigenic.⁶³ Despite binding preferentially the van der

(63) Schechter, I.; Sela, M. *Biochemistry* **1967**, *6*, 897.

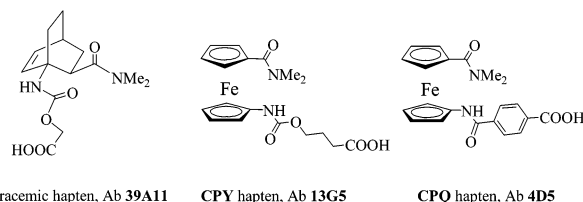


Figure 17. Racemic haptens used for generating Diels–Alderases that catalyze a similar transformation.

Waals complex between the reactants in the (*R,R*) configuration, these antibodies would catalyze the formation of the (*S,S*) product because of the particular distribution of hydrogen-bond donor and acceptor groups in the active site. This interpretation is in agreement with previous observations that not every antibody that binds the TSA will be an effective catalyst.⁶⁴ Screening for actual catalytic activity⁶⁵ rather than for TSA binding might help identify antibodies that enantioselectively catalyze the formation of each of the four diastereoisomeric Diels–Alder adducts.

The catalytic active site of Ab **13G5** consists of a deep hydrophobic pocket made of the variable domains (V_L and V_H) of the Fab. The polar residues that interact with the inhibitor and the transition states are located as follows: Tyr-L36 in the framework, at the border of the L1 loop, Asn-L91 in the L3 loop, Trp-H33 in the H1 loop, Asp-H50 in the H2 loop, and Thr-102 in the H3 loop. The sequence and size of these hypervariable regions or CDRs normally determine the specificity of the antibody–antigen interactions. Our results suggest that to further accelerate this reaction while maintaining the observed enantioselectivity, Tyr-L36 could be mutated to Lys. The perturbed pK_a of the side chain of lysine, that drops from 10.54 to 6.3–6.7 in a hydrophobic cavity,⁶⁶ would increase the strength of the hydrogen bond with *N,N*-dimethylacrylamide, further activating the dienophile toward the Diels–Alder reaction.

In the absence of antigen, the immune system presents an impressive diversity of antibodies (greater than 10^8 different binding sites).⁶⁷ Genetic and biochemical studies⁶⁸ have explained the origin of this sequence diversity of antibodies that derives from the combinatorial association of only 10^3 – 10^4 gene fragments. Once the immune system is challenged by an antigen, the process of affinity maturation provides further diversity by somatic mutation of the bases encoding for the variable region, leading to antibodies with increased affinity and specificity. In an effort to understand the immunological evolution of antibody catalysis, and ultimately, the structural basis for the transformation of sequence diverse antibodies into high affinity receptors,

several comparisons between germline and mature catalytic antibodies have been carried out. Particularly relevant to the present study is the case of antibody **39-A11**, that catalyzes a Diels–Alder reaction very similar to the one shown in Scheme 1. Structural and functional studies of the germline precursor suggest that **39-A11** and related antibodies (**DB3**, **TE33**, and **1E9**) derive from a family of germline genes that have been selected through evolution for the ability of the encoded proteins to form a polyspecific combining site (Figure 16).⁶⁹ Recent findings about the evolution of catalytic antibody **28B4** are also consistent with the notion that certain combinations of V_κ – J_κ and V_H give a polyspecific combining site which is to be tuned by CDR H3 for optimal specificity.⁷⁰ Analysis of hapten binding and catalytic determinants in a family of catalytic antibodies raised against a common TS analogue, which accelerate an oxy-Cope rearrangement, also revealed close homologies among the heavy chains of the catalytically active members, which derive mainly from a single germline gene.⁷¹ The light chains could be traced to several different but related germline genes. Construction and characterization of hybrid antibodies indicated a strong conservation of binding-site structure among the catalytically active clones. Finally, comparison of X-ray structures of the binding sites of catalytic antibodies raised to bind different phosphonates showed that, despite their different sequences, they all exhibit a tetrahedral array of hydrogen-bond donors complementary to the tetrahedral anion.⁷²

Despite the fact that **13G5** and **4D5** derive from immunization with the same mixture of racemic diastereoisomeric haptens, their sequences show only 40% homology (Figure 16). More surprising is the fact that neither of them evolves from the germline of antibody **39-A11**, despite the important structural similarity of the haptens (Figure 17).

These observations suggest that each hapten (**CPY** and **CPQ**, Figure 1b), and the hapten used to elicit **39-A11** (Figure 17) are recognized by different germline antibodies during the primary response. The different polar groups present in the CDRs of antibodies **13G5**, **4D5**, and **39A11** suggest that through selection and mutation, nature found different ways to catalyze the same chemical transformation.

Acknowledgment. We are grateful to the National Institute of General Medical Sciences, National Institutes of Health (GM61402 to K.N.H. and GM43858 to K.D.J.), the National Science Foundation (CHE-9616772 to K.N.H.), and The Skaggs Institute for Chemical Biology (K.D.J.) for financial support of this research.

Supporting Information Available: Experimental details (PDF). X-ray crystallographic file in CIF format. This material is available free of charge via the Internet at <http://pubs.acs.org>.

JA020879D

- (64) Mader, M. M.; Bartlett, P. A. *Chem. Rev.* **1997**, *97*, 1281–1301.
 (65) (a) Benedetti, F.; Berti, F.; Flego, M.; Resmini, M.; Bastiani, E. *Anal. Biochemistry* **1998**, *256*, 67–73. (b) Shulman, H.; Eberhard, A.; Eberhard, C.; Ulitzur, S.; Keinan, E. *Bioorg. Med. Chem. Lett.* **2000**, *10*, 2353–2356 and references therein.
 (66) (a) Lee, J. K.; Houk, K. N. *Science* **1997**, *276*, 942–945. (b) Daopin, S.; Anderson, D. E.; Baase, W. A.; Dalhquist, F. W.; Matthews, B. W. *Biochemistry* **1991**, *30*, 11521.
 (67) Burton, D. R. *Acc. Chem. Res.* **1993**, *26*, 405–411.
 (68) (a) Burnet, F. M. In *The Clonal Selection Theory of Acquired Immunity*; Vanderbilt University Press: Nashville, TN, 1959; p 53. (b) Talmage, D. W. *Science* **1959**, *129*, 1649. (c) Lederberg, J. *Science* **1959**, *129*, 1649. (d) Tonegawa, S. *Nature* **1983**, *302*, 575. (e) French, D. L.; Laskov, R.; Scharff, M. D. *Science* **1989**, *244*, 1152.

- (69) Romesberg, F. E.; Spiller, B.; Schultz, P. G.; Stevens, R. C. *Science* **1998**, *279*, 1929–1933.
 (70) Yin, J.; Mundorff, E. C.; Yang, P. L.; Wendt, K. U.; Hanway, D.; Stevens, R. C.; Schultz, P. G. *Biochemistry* **2001**, *40*, 10764–10773.
 (71) Ulrich, H. D.; Schultz, P. G. *J. Mol. Biol.* **1998**, *275*, 95–111.
 (72) Tantillo, D. J.; Houk, K. N. *Chem. Biol.* **2001**, *535*–545.